remote sensing

MDPI

Article

Spatio-Temporal Assessment and Future Projection of Land Cover Dynamics in Savanna Woodlands of Sudan Using Machine Learning and CA–ANN Modeling

Emad H. E. Yasin [1,2,*], Milan Koreň [3] and Kornel Czimber [1]

[1] Institute of Geomatics and Civil Engineering, Faculty of Forestry, University of Sopron, Bajcsy-Zsilinszky u. 4, 9400 Sopron, Hungary; czimber.kornel@uni-sopron.hu
[2] Department of Forest Management, Faculty of forestry, University of Khartoum, Khartoum North 13314, Sudan
[3] Department of Forest Resource Planning and Informatics, Faculty of Forestry, Technical University in Zvolen, T. G. Masaryka 24, 960 01 Zvolen, Slovakia; milan.koren@tuzvo.sk
* Correspondence: emad.hassanelawadyasin@phd.uni-sopron.hu or emad.yasin@uofk.edu

Highlights

What are the main findings?

- Dense woodland declined substantially between 1995 and 2021, while semi-bare land expanded and became the dominant land cover class.
- Future projections (2034–2060) indicate persistent dominance of semi-bare land with moderate recovery of dense woodland.

What are the implications of the main findings?

- The results reveal concurrent processes of degradation and localized regeneration in a semi-arid woodland ecosystem.
- The combined use of Random Forest classification and CA–ANN modeling enables effective analysis of long-term land cover dynamics and future scenarios.

Abstract

Spatio-temporal analysis of land cover (LC) dynamics is essential for understanding landscape transformation in semi-arid woodland ecosystems. This study assessed historical and projected land cover changes in the Elnour Natural Forest Reserve (ENFR), Sudan, from 1995 to 2060. Historical maps for 1995, 2008, and 2021 were generated using a Random Forest classifier, while future scenarios for 2034, 2047, and 2060 were simulated using a Cellular Automata–Artificial Neural Network (CA–ANN) model. The results show that semi-bare land expanded from 23.1% in 1995 to 40.0% in 2021, while dense woodland declined from 26.7% to 15.7%, indicating substantial structural transformation of the landscape. Open woodland exhibited partial recovery, increasing to 39.9% in 2021. Future projections indicate a moderate increase in dense woodland to 23.8% by 2060; however, semi-bare land remains the dominant class, reflecting persistent landscape instability. These findings demonstrate the coexistence of degradation and localized regeneration processes in ENFR and highlight the importance of long-term monitoring of land cover dynamics in dryland environments. The study further shows that integrating machine learning classification with spatially explicit CA–ANN modeling provides an effective framework for analyzing historical trends and exploring potential future trajectories of land cover change in data-limited semi-arid regions.

Academic Editors: Min Huang, Daoye Zhu, Nengcheng Chen, Tengping Jiang and Orhan Altan

Received: 19 February 2026
Revised: 29 March 2026
Accepted: 30 March 2026
Published: 3 April 2026

Keywords: land cover change; Random Forest; CA–ANN modeling; land cover projection; savanna woodland; forest degradation; Sudan

1. Introduction

Land cover (LC) dynamics represent one of the most critical indicators of global environmental change because they directly influence biodiversity patterns, ecosystem structure, climate regulation, and the capacity of landscapes to deliver essential ecosystem services such as carbon storage, hydrological regulation, and soil conservation [1–4]. These dynamics arise from complex interactions between anthropogenic drivers, including agricultural expansion, fuelwood harvesting, overgrazing, and settlement growth, and natural processes such as climate variability and soil degradation [5–8]. Alterations in land cover can significantly modify microclimates, disrupt hydrological cycles, reduce soil fertility, and weaken ecosystem resilience, thereby triggering cascading impacts on ecological integrity and human livelihoods [2,9–12]. Consequently, understanding land cover trajectories is fundamental for sustainable land management, environmental policy development, and ecosystem conservation, particularly in environmentally vulnerable regions [13–15].

Across sub-Saharan Africa, especially in semi-arid and dryland ecosystems, land cover change is occurring at an accelerated rate due to recurrent droughts, nutrient-poor soils, rapid population growth, and persistent socio-economic pressures [6,7,16,17]. These drivers intensify woodland degradation, promote cropland expansion, increase fuelwood extraction, and lead to widespread conversion of natural vegetation. Such processes frequently result in vegetation loss, landscape fragmentation, and declining ecosystem service provision [4,5,16,18]. The resulting transformations undermine food security, reduce soil productivity, and weaken climate resilience, thereby increasing the vulnerability of rural communities that depend heavily on natural resources [3,7,8,10]. Despite their importance, systematic and long-term monitoring of land cover dynamics remains limited in many African drylands due to data scarcity, technical constraints, and limited institutional capacity [14,19–21].

In Sudan, savanna woodlands and protected areas constitute critical socio-ecological systems that support local livelihoods through the provision of fuelwood, fodder, and non-timber forest products, while also delivering key regulating services such as soil stabilization and water retention [1,8,22–26]. However, these woodland ecosystems have experienced substantial degradation over recent decades due to increasing anthropogenic pressure, including mechanized agriculture, overgrazing, unregulated wood extraction, and expanding settlements [16,27–31]. These pressures have led to a progressive decline in dense woodland cover and an expansion of degraded woodland, shrub-dominated areas, and bare land. Such changes threaten biodiversity, reduce carbon stocks, accelerate soil degradation, and increase vulnerability to climate extremes [4,18,25,32–34]. Despite these growing concerns, spatially explicit and long-term assessments of land cover dynamics remain scarce in Sudan's semi-arid savanna woodlands, particularly studies that integrate both retrospective analysis and future predictive modeling [8,14,19,20].

Recent advances in satellite-based Earth observation and machine learning techniques provide new opportunities to overcome long-standing monitoring limitations in data-scarce regions [14,35–39]. Cloud-based geospatial platforms facilitate the efficient processing of large multi-temporal datasets and enable reproducible analyses of long-term land cover dynamics [14,35,40,41]. Among machine learning approaches, the Random Forest (RF) classifier has demonstrated strong performance due to its robustness to noisy data, ability to capture complex non-linear relationships, and high classification accuracy with rela-

tively low parameterization requirements [42–45]. Previous studies have shown that RF consistently produces reliable land cover classifications across heterogeneous dryland environments [14,43,45–47].

Beyond historical mapping, modeling future land cover trajectories is essential for anticipating ecological risks and supporting sustainable land-use planning [48–50]. The Cellular Automata–Artificial Neural Network (CA–ANN) framework is particularly effective for simulating spatial dynamics of land cover change, as it integrates historical transition patterns with neural network–derived transition rules to capture both spatial dependence and non-linear processes [51–59]. When applied to accurately classified land cover datasets, CA–ANN enables the generation of spatially explicit projections that can reveal potential pathways of woodland degradation, persistence, or recovery under evolving environmental and socio-economic conditions [14,38,39,47,60].

Previous land cover studies in Sudan have largely relied on conventional classification approaches, such as maximum likelihood applied to Landsat or ASTER imagery, to document historical changes [5,16,18,27,61–66]. While these studies provide valuable insights into vegetation decline and land degradation, they are often limited to retrospective analyses and do not incorporate predictive modeling or advanced machine learning techniques. Furthermore, integrated frameworks that combine multi-temporal classification with spatially explicit simulation remain scarce, particularly in savanna woodland ecosystems where ecological pressures are intensifying [8,14,19,20].

The Elnour Natural Forest Reserve (ENFR) in Blue Nile State represents a critical example of a semi-arid savanna woodland system undergoing rapid transformation due to illegal logging, intensive grazing, and localized agricultural expansion [8,16,18,65,66]. Understanding the spatio-temporal dynamics of land cover change in this region, as well as its potential future trajectories, is essential for informing sustainable management and conservation strategies.

Therefore, this study aims to (i) quantify multi-temporal land cover dynamics in the ENFR savanna woodlands using a Random Forest classifier, and (ii) simulate future land cover changes using a CA–ANN modeling framework. By integrating long-term satellite observations with spatially explicit predictive modeling, this research provides a comprehensive assessment of landscape transformation in a data-limited dryland environment. The study contributes to advancing understanding of woodland degradation processes, improving predictive capacity for land cover change, and supporting evidence-based decision making for sustainable woodland management and restoration planning in Sudan and similar semi-arid regions.

2. Materials and Methods

2.1. Study Area

This study was conducted in Blue Nile region at Elnour Natural Reserve Forest (ENFR), located between longitudes 11°48′19″N and 11°53′30″N and latitudes 34°28′47″E and 34°32′35″E, 6 km southeast of El Damazin Town and about 3 km east of El Rosaries town. The forest was declared as a reserved forest on 15 June 1959, covering a total area of 4667.17 ha to offer high degree of protection from poaching, and hunting for biodiversity conservation (Figure 1). The region's climate is tropical and subcontinental characterized by humid rainy summers and dry winters. The temperature during winter months (December–January) ranges from 16.41 °C to 15.62 °C, while in summer (April and May) can reach 41.48 °C to 39.91 °C. A significant change in mean daily temperature occurs during the rainy period from June to October due to high humidity. Additionally, rainfall is influenced by South Atlantic and Congo air masses, with minimal impact from the Indian Ocean as well as precipitation varies between 300–700 mm from April to November,

peaking from July to September. Harison and Jackson [67] classified Sudan's vegetation into various categories, with ENFR classified as low rainfall woodland savannah, featuring 55 woody plant species from 36 genera and 18 families [68]. Dominant species in the reserve include *Sterculia setigera* Delile, *Combretum hartmannianum* Schweinf., *Acacia seyal* (Delile), *Terminalia brownii* Fresen., *Terminalia laxiflora* Engl., *Anogeissus leiocarpus* (DC.) Guill. & Perr., *Balanites aegyptiaca* (L.) Delile, *Combretum micranthum* G.Don, and *Lannea fruticosa* (Hochst. ex A.Rich.) Engl. [69]. The reserve also contains ecologically important and threatened species such as *Adansonia digitata* L., *Boswellia papyrifera* (Delile) Hochst., *Dalbergia melanoxylon* Guill. & Perr., *Grewia* spp., *Lonchocarpus laxiflorus* Guill. & Perr., *Piliostigma reticulatum* (DC.) Hochst., and *Xeromphis nilotica* (Stapf) Keay [70]. The topography of ENFR is slightly flattened, with some depressions in the central and northern clay areas [71]. The reserve forest soil is classified into two types: dark cracking clay soil, constituting about 64.2% of the forest area (2994.31 ha), and sandy loam to gravelly soil covering 35.8% (1672.86 ha). El Azaza is the nearest village to the reserve forest, part of Hamag civil administration under Mayer Obied Abou Shotal, that inhabits main tribes including Kenana (Arab), Rufaa (Arab), Bargo, Masalit, Fallata, Dinka, El Broon, and Tama. The village inhabitants periodically collect dry branches and twigs for firewood, as well as fruits, leaves, barks, and roots for medicine and building materials for life sustenance. The forest serves as a grazing area during the dry season from March to May, except where new regeneration is established.

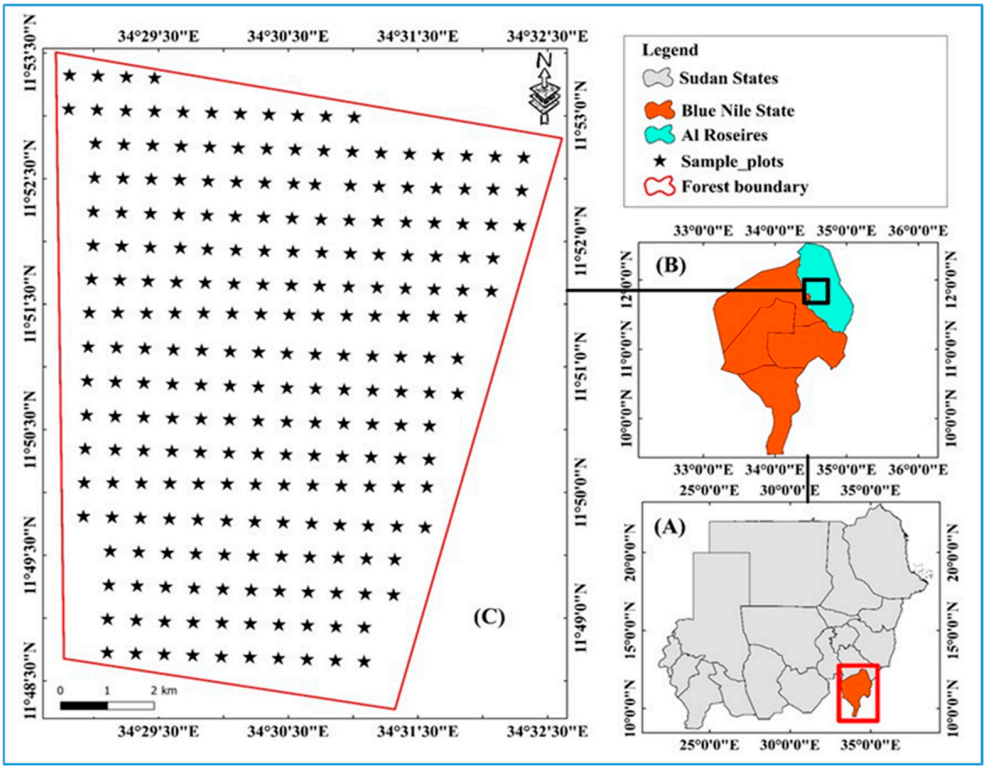

Figure 1. Spatial distribution of sampling plots in the Elnour Natural Forest Reserve (ENFR), Blue Nile State, Sudan. (**A**) Location of the study area within Sudan. (**B**) Regional location within Blue Nile State (Al Roseires locality). (**C**) Distribution of sampling plots within the forest boundary.

2.2. Data Collection and Preprocessing

Figure 2 illustrates the methodological workflow adopted in this study. Landsat multispectral imagery remains a cornerstone for long-term land cover (LC) time series analysis due to its extensive historical archive and consistent spectral properties [72]. In this study, multi-temporal datasets from Landsat 5 Thematic Mapper (TM) (30 m) and

Sentinel-2 (10 m) were obtained from the Google Earth Engine (GEE) open-access catalog within the WGS84 reference system [35].

The integration of Landsat and Sentinel-2 data was motivated by the need to ensure temporal continuity while benefiting from improved spatial resolution in recent years. To minimize inconsistencies arising from sensor differences, all datasets were harmonized through radiometric calibration, atmospheric correction, and spatial resampling to a common resolution prior to analysis.

Comprehensive preprocessing included cloud masking, atmospheric and topographic corrections, geometric alignment, and layer stacking. For each target year (1995, 2008, and 2021), annual median composites were generated using imagery acquired between 1 January and 31 December, following established approaches to reduce noise and seasonal variability in multi-temporal analyses [40,41].

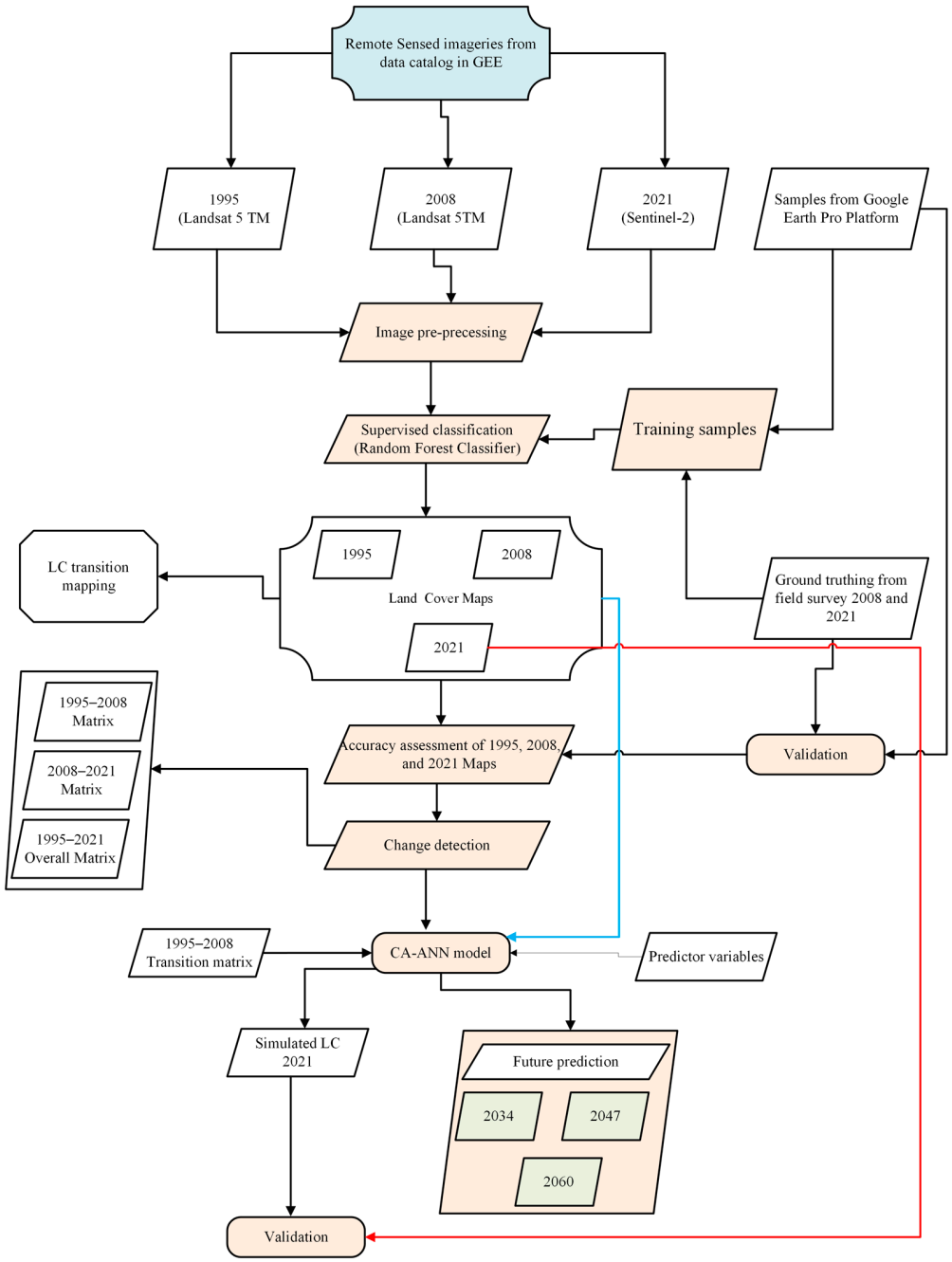

Figure 2. Schematic workflow for data collection and analysis.

2.3. Training and Testing Data for the Classification Algorithm

Accurate land cover mapping requires assigning each pixel to a predefined class, a process influenced by classifier selection, training data quality, and reference data reliability [30,35,40]. In this study, four land cover classes: bare land, semi-bare land, open woodland (formerly light forest), and dense woodland, were mapped for 1995, 2008, and 2021 (Table 1). These classes were defined based on canopy cover thresholds and ecological characteristics derived from previous studies [36], field observations, and expert knowledge. Representative field photographs illustrating the structural characteristics of each land cover class are provided in Figure 3, supporting the interpretation of classification categories based on canopy cover thresholds.

Table 1. Definition of land cover (LC) classes used in this study.

No.	Land Cover Classes	Class Description
1	Bare land (BL)	Areas with no vegetation cover consisting of exposed soils
2	Semi-bare land (SBL)	Areas covered by less than 10% of tree canopy
3	Open Woodland (OWL)	Areas covered at least 10% and less than 40% of tree canopy
4	Dense Woodland (DWL)	Areas covered by more than 40% of tree canopy

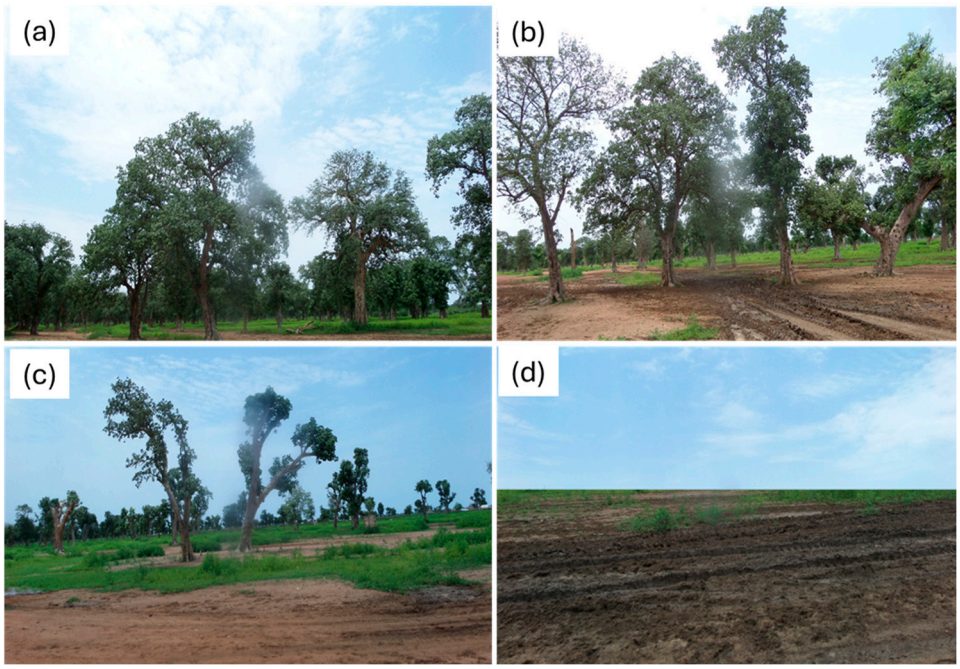

Figure 3. Representative field photographs of land cover classes in the Elnour Natural Forest Reserve (ENFR): (**a**) dense woodland, (**b**) open woodland, (**c**) semi-bare land, and (**d**) bare land.

Reference samples were collected from two field campaigns (2008 and 2021; 229 samples each) and supplemented by onscreen digitization of high-resolution imagery in Google Earth Pro. This approach is widely recognized for generating reliable training data in remote sensing studies [39,45,73].

A total of 916 samples per reference year were compiled (687 from onscreen interpretation and 229 from field data) and proportionally distributed across classes. Of these, 70% (641 samples) were used for training the Random Forest classifier. Training polygons were designed to be spatially homogeneous and limited in size to reduce spatial autocorrelation and capture intra-class spectral variability.

The remaining 30% (275 samples) were reserved for independent validation. Test samples were randomly distributed and maintained at a minimum distance of 100 m from

training samples to avoid spatial dependence and ensure unbiased accuracy assessment [73] (Appendix A Table A1).

2.4. Landsat and Sentinel-2 Images Classification

Supervised classification of land cover was performed using the Random Forest (RF) algorithm, a non-parametric ensemble learning method widely applied in remote sensing for handling high-dimensional and heterogeneous datasets [74]. The RF classifier was applied to multi-temporal Landsat and Sentinel-2 imagery to map four land cover classes in the ENFR, Blue Nile State, Sudan.

The selection of RF was based on its demonstrated capability to model complex, non-linear relationships between spectral variables and land cover classes, as well as its robustness to noise and overfitting [43,47,75]. RF constructs multiple decision trees using bootstrap samples of the training dataset and aggregates their outputs through majority voting to assign the final class label [9,42]. This ensemble approach improves classification stability and generalization, particularly in environments characterized by spectral variability.

The model was parameterized following established practices [9,46], using 100 decision trees (ntree = 100), while the number of variables randomly selected at each split (mtry) was set to the square root of the total number of predictor variables. These parameter settings provide a balance between computational efficiency and predictive performance.

The suitability of RF for this study is further supported by its ability to handle large datasets, reduce sensitivity to outliers, and maintain stable performance across different land cover types, making it appropriate for multi-temporal classification of savanna woodland environments [39,45,76].

2.5. Classification Accuracy Assessment

The reliability of any thematic LULC map depends on both its overall accuracy and the class-specific accuracy of individual land-cover categories [77]. Accuracy assessment typically employs several well-established metrics, including overall accuracy (OA), producer's accuracy (PA), and user's accuracy (UA) (Appendix A Table A2). In this study, we computed OA, PA, and UA for each reference year, excluding kappa coefficient due to its widely documented limitations in reflecting true map reliability [78].

To provide a more robust, class-specific measure of accuracy, we also calculated the F1-score, which synthesizes *PA* and *UA* into a single metric ranging from 0 to 100% [79]. The *F1-score* for class *i* was computed as:

$$F1_i = \frac{2 \times PA_i \times UA_i}{PA_i + UA_i} \quad (1)$$

Given ongoing concerns regarding the interpretability and statistical weaknesses of the kappa coefficient in thematic accuracy evaluation [78], we further incorporated two complementary disagreement metrics: quantity disagreement (QD) and allocation disagreement (AD), as proposed by Pontius and Millones [80]. QD quantifies discrepancies between the observed and predicted class proportions, whereas AD captures differences in the spatial allocation of predicted versus observed samples. Together, these metrics offer a more nuanced and reliable characterization of classification performance.

2.6. LC Change Detection

LC dynamics across the study area were quantified by analyzing classified maps from multiple time slices. The proportional change in each LULC category was computed following the approach in [81] using:

$$C = \frac{C_2 - C_1}{C_1} \times 100 \quad (2)$$

where C_1 and C_2 denote the area of each LULC class in the baseline year (1995) and the terminal year (2021), respectively.

To further elucidate landscape trajectories, a transition matrix was generated to characterize LULC stocks, their composition, and net gains or losses. Additionally, LULC transitions among classes were evaluated at 13-year intervals, 1995–2008, 2008–2021, and overall change 1995–2021, to capture the direction, magnitude, and persistence of class-to-class transformations throughout the study period.

2.7. LC Transition Mapping

To visualize and quantify the spatiotemporal dynamics of land use/land cover (LULC) transitions in ENFR, we generated transition maps and matrices using ArcGIS Pro 3.6, following established LULC transformation assessment approaches [10,82]. Classified LULC maps from 1995, 2008, and 2021 served as reference layers for detecting class-to-class conversions across the study period. These datasets enabled the derivation of transition pathways over 13-year and 26-year intervals, thereby capturing both short-term and long-term landscape transformations and providing a comprehensive overview of LULC change trajectories.

2.8. Future Prediction of LC

Future land cover (LC) projections were performed using a hybrid Cellular Automata–Artificial Neural Network (CA–ANN) modeling framework. Multi-temporal LC maps derived from Landsat imagery for 1995, 2008, and 2021 (13-year intervals) were used to characterize historical transitions and support future simulations. The CA–ANN model was implemented using the MOLUSCE plugin in QGIS (version 3.44.3), which is widely applied for spatio-temporal land cover analysis and scenario-based prediction of landscape dynamics [54,58,59,83,84].

The modeling framework was driven by a set of biophysical and accessibility-related predictors selected based on their relevance to land cover change processes and data availability [50,57,85]. These predictors included elevation, slope, aspect, distance to roads, and distance to streams (Appendix A Figure A1). Such variables are commonly used in land cover modeling as they provide spatially explicit representations of environmental constraints and human accessibility that influence landscape transitions [58]. All predictor layers were standardized and resampled to a common spatial resolution of 10 × 10 m in the WGS_1984_UTM_Zone_36N coordinate reference system prior to model implementation.

The CA–ANN framework integrates two complementary components:

(i) An Artificial Neural Network (ANN), which estimates transition suitability by modeling non-linear relationships between observed land cover changes and the selected driving factors.

(ii) A Cellular Automata (CA) module, which incorporates neighborhood configuration and spatial contiguity during the allocation of future land cover states.

Transition probability matrices were derived from observed changes between 1995 and 2008 and between 2008 and 2021. These matrices were used to parameterize the temporal dynamics of land cover transitions, while the ANN-generated suitability surfaces guided their spatial distribution.

Model validation was conducted by simulating the 2021 land cover map using transition probabilities derived from the 1995–2008 period and comparing the simulated output with the observed 2021 classification. Model performance was evaluated using the accuracy metrics provided by the MOLUSCE plugin, including overall accuracy (percent correct-

ness), Kappa for location, and Kappa for histograms, enabling assessment of both spatial agreement and class distribution consistency.

Following validation, the calibrated CA–ANN model was applied to simulate future land cover scenarios for 2034, 2047, and 2060. Transition probability matrices (P_{ij}) were computed based on observed transitions and combined with ANN-derived suitability maps and CA neighborhood rules. Future land cover states were estimated using the Markov transition framework [86]:

$$S(t+1) = P_{ij} \times S(t) \quad (3)$$

where $S(t)$ and $S(t+1)$ represent the LULC states at time t and $t+1$, respectively, and P_{ij} denotes the probability of transition from class i to class j, subject to the constraint [87]:

$$0 \leq P_{ij} \leq 1 \quad (4)$$

The transition matrices, combined with ANN-generated suitability maps and CA spatial allocation rules, were used to generate the final LULC projections for 2034, 2047, and 2060.

3. Results

3.1. Land Cover Results for 2021

The 2021 Sentinel-2 classification identified four primary land cover classes in ENFR: dense woodland (15.7%), open woodland (39.9%), semi-bare land (40.0%), and bare land (4.4%) (Figure 4; Table 2). Semi-bare land represents the dominant class, covering approximately 40% of the study area, followed closely by open woodland. When combined, semi-bare land and bare land account for 44.4% of the reserve, indicating a substantial proportion of sparsely vegetated or exposed land surfaces. In contrast, dense woodland occupies a relatively limited extent, representing only 15.7% of the total area, while open woodland forms the most extensive vegetated class. Overall, the land cover composition in 2021 is characterized by the dominance of intermediate- and low-density vegetation, with comparatively limited areas of dense woodland.

Table 2. Land cover (LC) changes in ENFR (1995–2021): area and percentage.

Class	1995		2008		2021	
	Area (ha)	%	Area (ha)	%	Area (ha)	%
Bare land	242.6	5.1	297.2	6.3	206.3	4.4
Semi-bare land	1091.0	23.1	1788.5	37.8	1893.8	40.0
Open Woodland	2132.6	45.1	1500.2	31.7	1887.9	39.9
Dense Woodland	1264.9	26.7	1145.2	24.2	743.2	15.7
Total	4731.1	100	4731.1	100	4731.1	100

3.2. Land Cover (LC) Dynamics in ENFR (1995–2021)

Analysis of land cover dynamics in ENFR for the years 1995, 2008, and 2021 (Figure 3; Table 2) reveals substantial temporal changes across all classes. Bare land increased from 5.1% in 1995 to 6.3% in 2008, followed by a decline to 4.36% in 2021. Semi-bare land exhibited the most pronounced expansion, increasing from 23.1% in 1995 to 37.8% in 2008 and further to 40.0% in 2021, becoming the dominant land cover class. Open woodland declined markedly from 45.1% in 1995 to 31.7% in 2008, before recovering to 39.9% in 2021. In contrast, dense woodland showed a continuous decline throughout the study period, decreasing from 26.7% in 1995 to 15.7% in 2021. These patterns indicate a shift in land cover composition characterized by the expansion of semi-bare land and the reduction in dense woodland, accompanied by partial recovery of open woodland between 2008 and 2021.

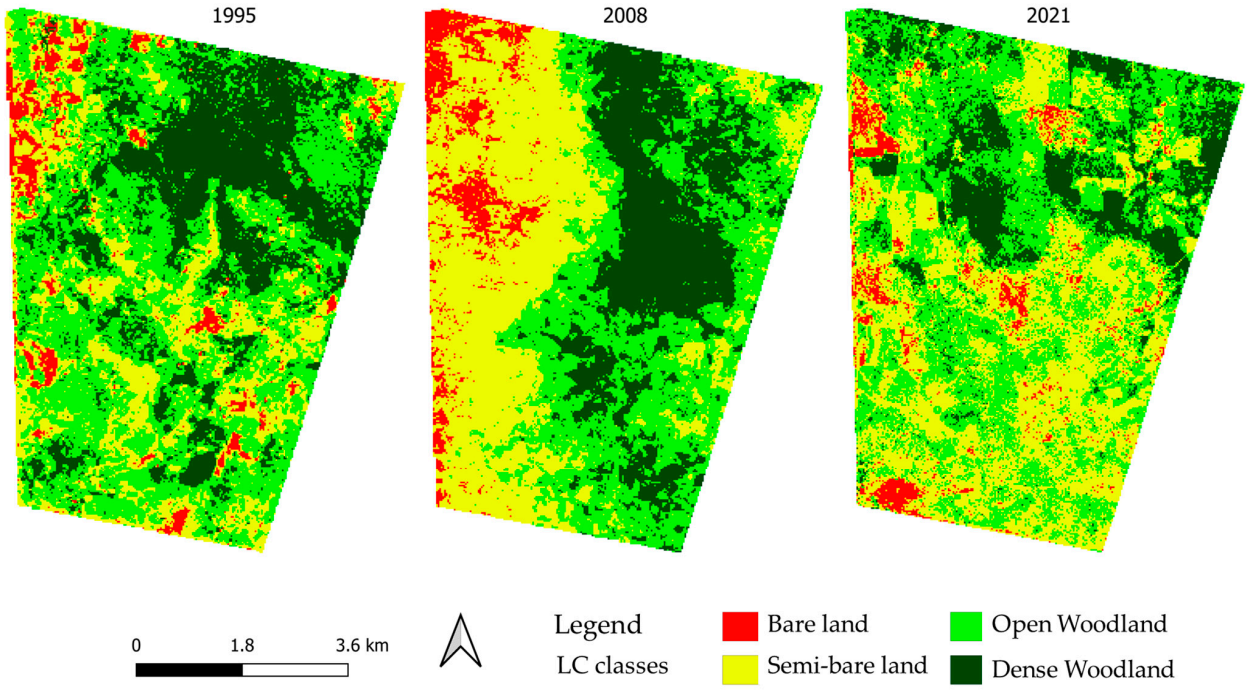

Figure 4. Land cover change maps of ENFR between 1995 and 2021.

3.3. Land Cover Change Trajectories

Land cover transitions in ENFR were analyzed using transition matrices (Table 3) and spatial maps (Figure 5) for the periods 1995–2008, 2008–2021, and 1995–2021. Between 1995 and 2008, dense woodland exhibited low persistence (10.9%), with major transitions to open woodland (9.7%) and semi-bare land (3.3%). Semi-bare land expanded substantially (Δ + 14.7%), primarily through conversions from open and dense woodland. Open woodland retained 14.3% of its area while transitioning significantly to semi-bare land (18.5%) and dense woodland (8.6%), indicating simultaneous redistribution among vegetation classes. Bare land showed minimal persistence (1.0%) and was redistributed among other classes. During 2008–2021, dense woodland persistence declined further to 3.5%, with most transitions occurring toward semi-bare land (11.1%) and open woodland (8.9%). Semi-bare land remained dominant (Δ + 2.3%), expanding mainly at the expense of vegetated classes. Open woodland showed moderate persistence (13.1%) and gains from semi-bare land (15.2%), while bare land remained highly dynamic (0.4%). Over the full period (1995–2021), semi-bare land recorded a net increase of approximately 17%, becoming the dominant class, while dense woodland declined by 11% and open woodland decreased by 5.2%. Bare land showed a minor net decrease (−0.7%), acting primarily as a transitional class. These transitions indicate substantial redistribution of land cover classes over time, with dominant flows from vegetated classes toward semi-bare land.

Table 3. Land cover (LC) transition matrices in ENFR between 1995 and 2021 (in %). Columns represent the land cover class at the start of the period; Raws represent the land cover class at the end.

Period	From/To	Bare Land	Semi-Bare Land	Open Woodland	Dense Woodland	End %
1995–2008	Bare land	1.0	2.1	2.7	0.6	6.3
	Semi-bare land	2.7	9.9	18.5	6.7	37.8
	Open Woodland	1.0	7.8	14.3	8.6	31.7
	Dense Woodland	0.4	3.3	9.7	10.9	24.2
	Start %	5.1	23.1	45.1	26.7	100

Table 3. *Cont.*

Period	From/To	Bare Land	Semi-Bare Land	Open Woodland	Dense Woodland	End %
2008–2021	Bare land	0.4	2.5	0.7	0.8	4.4
	Semi-bare land	2.3	13.3	13.4	11.1	40.1
	Open Woodland	2.6	15.2	13.1	8.9	39.8
	Dense Woodland	1.0	6.8	4.4	3.5	15.7
	Start %	6.3	37.8	31.6	24.3	100
1995–2021	Bare land	0.6	1.5	1.6	0.7	4.4
	Semi-bare land	2.2	10.9	18.3	8.6	40
	Open Woodland	1.6	8.6	17.9	11.7	39.9
	Dense Woodland	0.7	2	7.2	5.8	15.7
	Start %	5.1	23.1	45.1	26.8	100

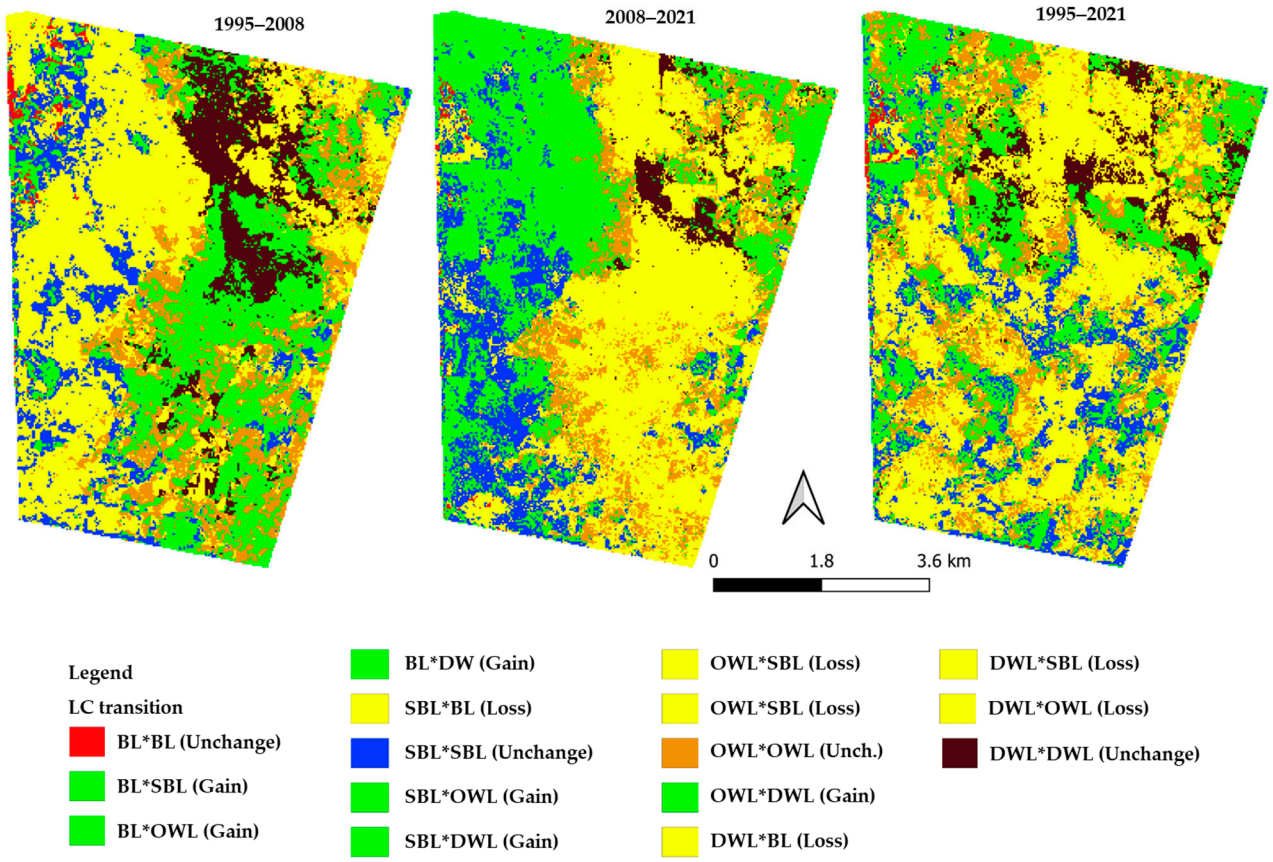

Figure 5. Land cover (LC) change trajectories in ENFR from 1995 to 2021 derived from transition matrix analysis, where col-ors indicate transition categories (gain, loss, and unchanged) rather than individual class-to-class changes.

3.4. Trend Analysis of ENFR Condition During 1995–2021

Trend analysis of ENFR land cover from 1995 to 2021 (Figure 6) shows distinct temporal patterns across classes. Bare land increased by 24.9% (+1.92% annually) during 1995–2008, followed by a decrease of 25.7% (−1.98% annually) during 2008–2021, resulting in a near-stable overall change (−0.8%, −0.03% annually). Semi-bare land decreased slightly during 1995–2008 (−1.9%, −0.15% annually), then increased substantially during 2008–2021 (+18.9%, +1.45% annually), yielding a net increase of 17.0% (+0.65% annually). Open woodland declined by 20.6% (−1.58% annually) during the first period, followed by an increase of 15.4% (+1.45% annually) in the second period, resulting in a net decrease of 5.2%. Dense woodland showed a consistent decline, decreasing by 2.4% (−0.18% annually)

during 1995–2008 and by 8.6% (−0.66% annually) during 2008–2021, with a total reduction of 11.0% (−0.84% annually). Overall, these trends indicate increasing dominance of lower-density land cover classes and a reduction in dense woodland cover over time.

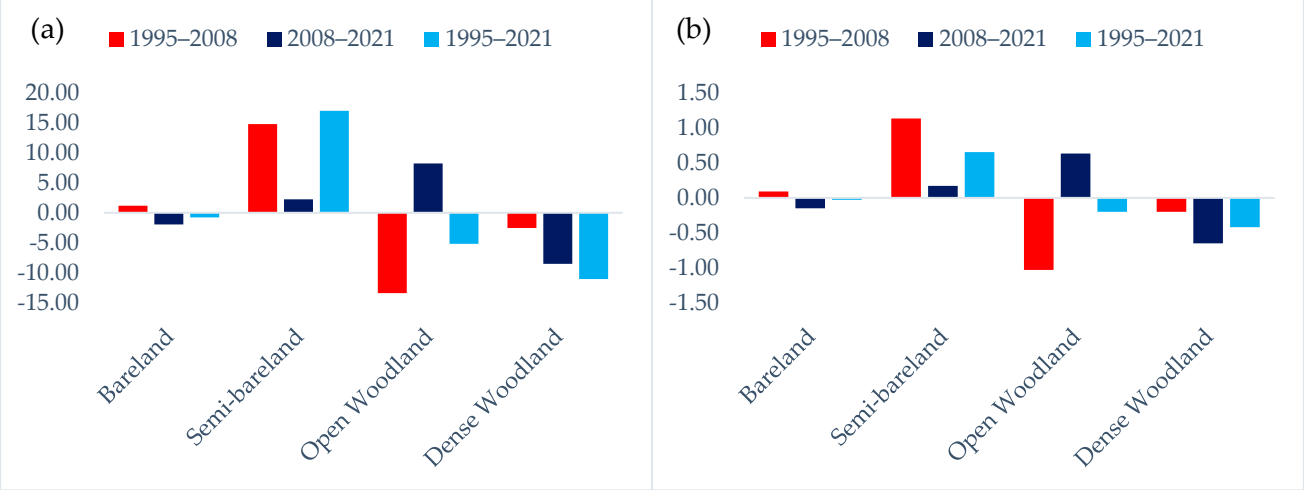

Figure 6. Spatiotemporal dynamics of LC change in the ENFR between 1995 and 2021: (**a**) trend direction of change, (**b**) annual rate of change.

3.5. Future Land Cover Prediction

Projected land cover in ENFR for 2034, 2047, and 2060 shows distinct temporal trajectories based on modeled transitions (Figure 7; Table 4). Bare land increases from 5.6% in 2034 to 8.8% in 2047, followed by a slight decrease to 8.0% in 2060. Semi-bare land remains the dominant class, decreasing from 37.1% in 2034 to 28.6% in 2047 and stabilizing at 28.9% in 2060. Open woodland remains relatively stable, ranging between 34.5% and 34.0% throughout the projection period. Dense woodland shows a continuous increase, expanding from 22.8% in 2034 to 29.1% in 2060. Overall, the projections indicate persistence of semi-bare land dominance, stability of open woodland, moderate fluctuation in bare land, and gradual increase in dense woodland.

Table 4. Projected Land cover (LC) changes in ENFR (2034–2060): area and percentage.

Class	2034		2047		2060	
	Area (ha)	%	Area (ha)	%	Area (ha)	%
Bare land	265.3	5.6	417.8	8.8	377.7	8.0
Semi-bare land	1757.1	37.1	1350.9	28.6	1366.4	28.9
Open Woodland	1631.0	34.5	1611.7	34.1	1610.0	34.0
Dense Woodland	1077.7	22.8	1350.8	28.6	1377.0	29.1
Total	4731.1	100	4731.1	100	4731.1	100

3.6. Trend Analysis of ENFR Condition During 2047–2060

Projected trends from 2034 to 2060 (Figure 8) show varying patterns across land cover classes. Bare land increases by 3.2% (+0.25% annually) during 2034–2047, followed by a decrease of 0.85% (−0.07% annually) during 2047–2060, resulting in a net increase of 2.37% (+0.09% annually). Semi-bare land decreases by 8.6% (−0.66% annually) between 2034 and 2047, followed by a slight increase of 0.33% (+0.03% annually), yielding a net decrease of 8.3% (−0.32% annually). Open woodland shows a minor overall decline of 0.44% (−0.02% annually), while dense woodland increases by 6.3% (+0.24% annually). These trends indicate a reduction in semi-bare land and gradual expansion of dense woodland, with relatively stable patterns in other classes.

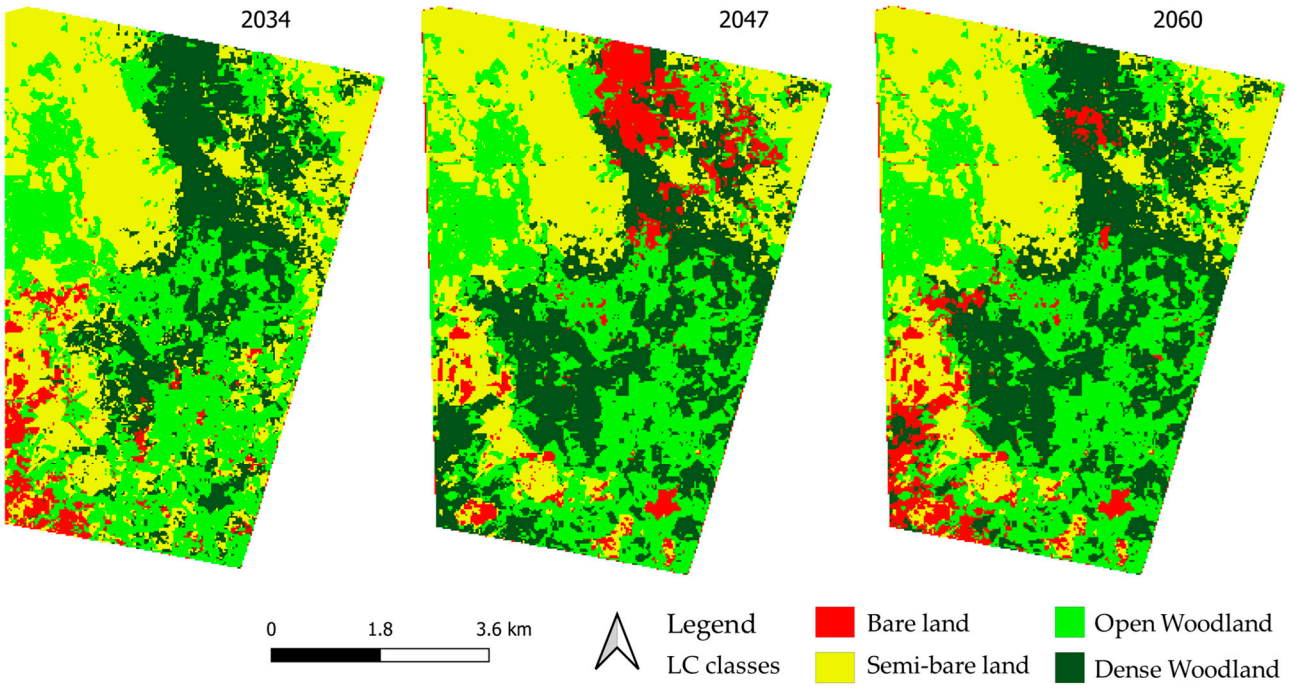

Figure 7. Future projection of land cover change maps of ENFR between 2034–2060.

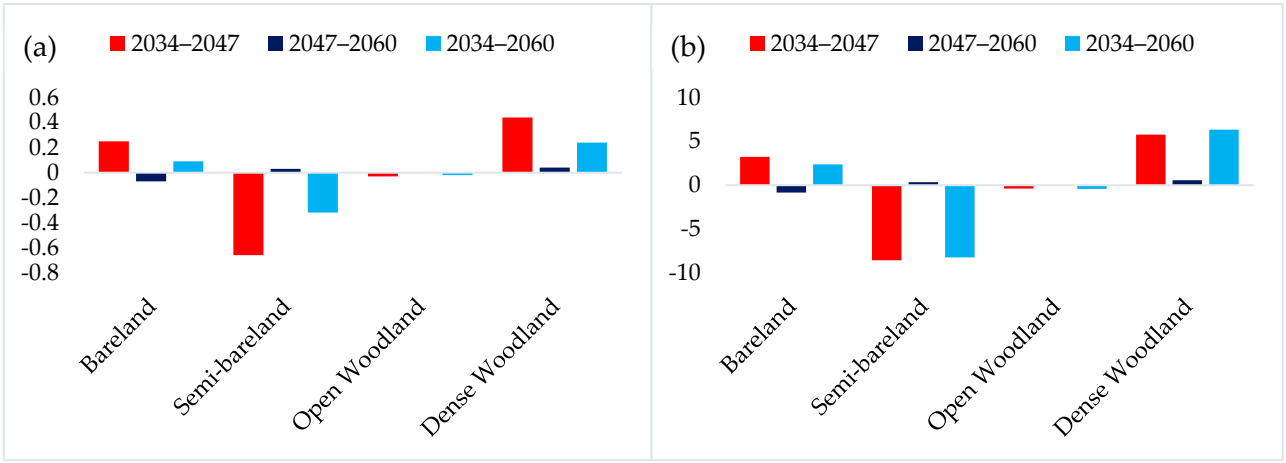

Figure 8. Spatiotemporal dynamics of LC change in the ENFR between 2034 and 2060: (**a**) trend direction of change, (**b**) annual rate of change.

3.7. Future Land Cover Change Trajectories

Future land cover transitions were analyzed using transition matrices (Table 5) and spatial maps (Figure 9). Between 2021 and 2034, dense woodland persistence is low (4.1%), with major transitions to open woodland (10.5%) and semi-bare land (7.7%). Open woodland retains 9.3% of its area and gains from semi-bare land (22.7%) and dense woodland (10.5%). Semi-bare land shows moderate persistence (6.9%) and transitions toward vegetated classes, while bare land remains minimal (0.6%). During 2034–2047, dense woodland persistence increases to 15.2%, while semi-bare land remains dominant (28.0%) and open woodland persists at 32.1%. From 2047–2060, dense woodland persistence increases further to 23.8%, with continued gains from other classes. Open woodland remains stable (33.6%), and semi-bare land persists at 28.1%, while bare land continues transitioning into vegetated classes. Overall, the results indicate ongoing redistribution among land cover classes, with increasing persistence of dense woodland and continued dominance of semi-bare land.

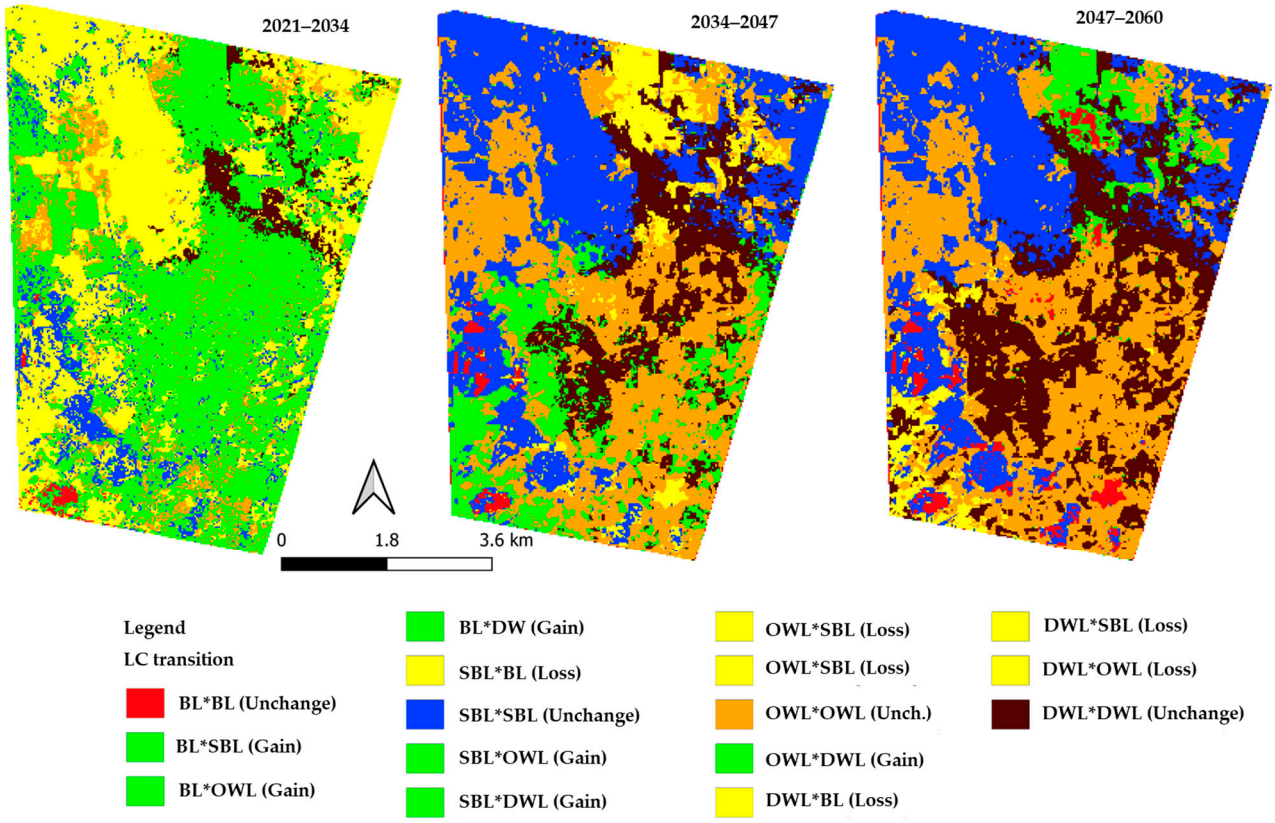

Figure 9. Projected land cover change trajectories in ENFR from 2021 to 2060 derived from transition matrix analysis, where colors indicate transition categories (gain, loss, and unchanged) rather than individual class-to-class changes.

Table 5. Projected Land cover (LC) change transition matrices in ENFR between 2021 and 2060 (in %). Columns represent the land cover class at the start of the period; Raws represent the land cover class at the end.

Period	From/To	Bare Land	Semi-Bare Land	Open Woodland	Dense Woodland	End %
2021–2034	Bare land	0.6	2.7	2.1	0.2	5.6
	Semi-bare land	1.6	6.9	18.1	10.6	37.1
	Open Woodland	1.6	22.7	9.3	0.9	34.5
	Dense Woodland	0.5	7.7	10.5	4.1	22.8
	Start %	4.4	40	39.9	15.7	100
2034–2047	Bare land	1.1	0.4	0.8	6.4	8.8
	Semi-bare land	0.0	28.0	0.1	0.4	28.6
	Open Woodland	0.3	1.0	32.1	0.8	34.1
	Dense Woodland	4.2	7.8	1.4	15.2	28.6
	Start %	5.6	37.1	34.5	22.8	100
2047–2060	Bare land	3.8	0.2	0.2	3.9	8
	Semi-bare land	0.1	28.1	0.1	0.6	28.9
	Open Woodland	0.1	0.1	33.6	0.2	34
	Dense Woodland	4.9	0.2	0.2	23.8	29.1
	Start %	8.8	28.6	34.1	28.6	100

3.8. CA–ANN Model Validation

To assess the reliability of the CA–ANN model, the simulated 2021 land cover map was compared with the observed classification for the same year (Figure 10). The comparison

shows strong spatial agreement between the two maps, particularly for dominant classes such as semi-bare land and open woodland. Dense woodland areas are also well represented, although minor discrepancies occur along class boundaries and transition zones. These differences are expected due to the stochastic nature of the model and the complexity of land cover transitions. Overall, the model effectively reproduces the spatial distribution of major land cover classes, supporting its application for future LULC projections.

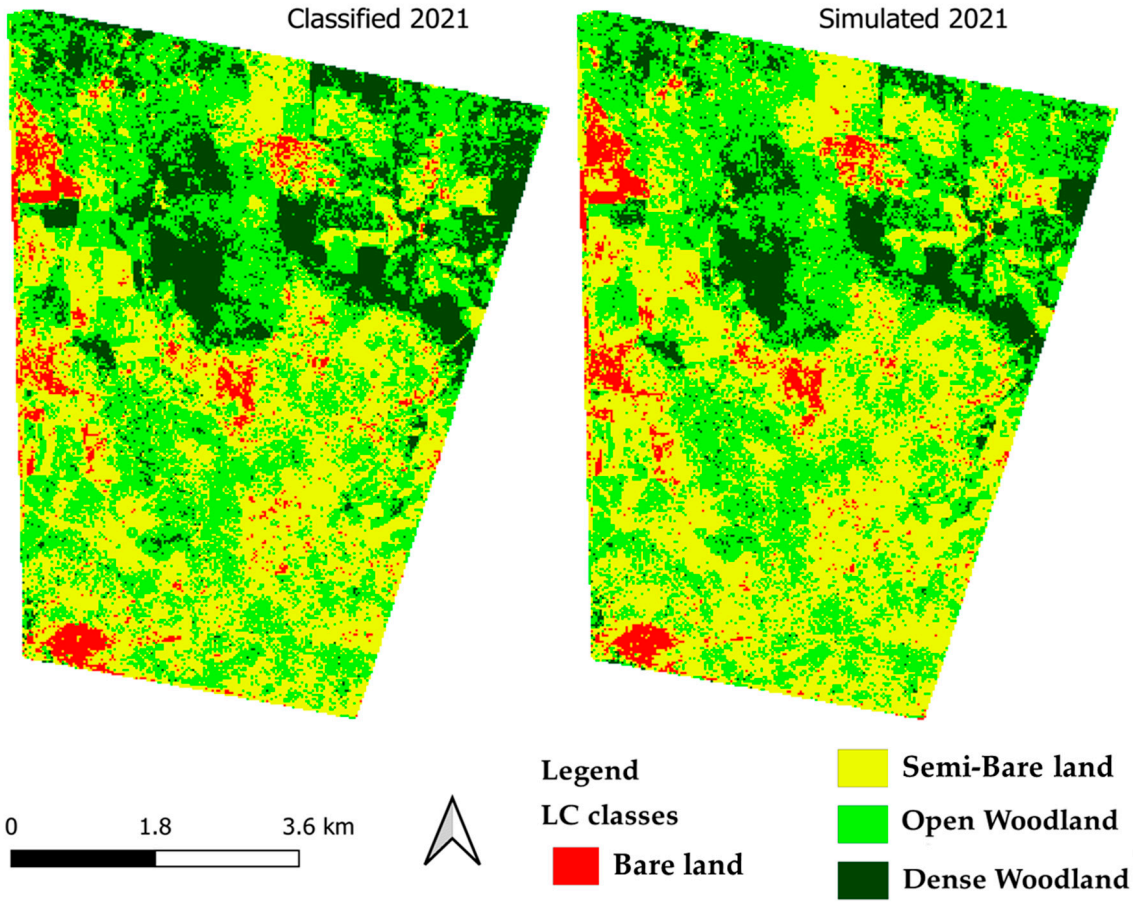

Figure 10. Comparison between observed (classified) and simulated 2021 land cover maps used for validation of the CA–ANN model in the Elnour Natural Forest Reserve (ENFR).

3.9. Drivers of Forest Degradation in ENFR

The assessment of drivers of woodland degradation in the Elnour Natural Forest Reserve (ENFR) was based on field observations, expert consultation, and evidence from previous studies conducted in similar dryland ecosystems of Sudan [8,16,18,65,66]. The relative importance of each driver was evaluated using a semi-quantitative approach considering the frequency, spatial extent, and observed intensity of disturbances within the study area.

The results in Table 6 indicate that anthropogenic drivers dominate the degradation process. Illegal tree cutting and charcoal production were identified as the most significant drivers, with widespread occurrence across the study area and clear evidence of mature tree removal. Overgrazing was also observed extensively, particularly along livestock movement routes, where reduced seedling density and limited regeneration were recorded.

Governance-related factors, including weak enforcement and limited institutional capacity, were consistently associated with areas experiencing intensive resource extraction. Similarly, socioeconomic dependence on woodland resources was observed to contribute to continuous pressure on vegetation, particularly in zones closer to settlements.

Table 6. Relative importance of drivers of woodland degradation in ENFR.

Driver Category	Specific Driver	Relative Importance	Evidence Type
Human-Induced	Illegal tree cutting and charcoal production	Very High	Field observation, literature
	Overgrazing by livestock	High	Field observation
	Weak governance and enforcement	Moderate	Institutional assessment, literature
	Socioeconomic dependence	Moderate	Field observation, literature
	Agricultural expansion and settlement	Moderate–Low	Land cover change detection
Environmental	Climatic variability (rainfall and drought)	Low–Moderate	Climate pattern observation, literature
Ecological Consequences	Fragmentation and species composition changes	Very Low	Long-term result of persistent human and climatic pressures.

Land-use expansion, mainly in the form of small-scale agriculture and settlement development, was detected in localized areas, resulting in permanent conversion of woodland to non-vegetated or cultivated land. In addition, environmental factors such as prolonged dry seasons and irregular rainfall patterns were observed to influence vegetation conditions, particularly by reducing regeneration success in degraded areas.

The combined influence of these drivers is reflected in the observed land cover transitions, including the reduction in dense woodland, expansion of open woodland and semi-bare land, and increased landscape fragmentation.

4. Discussion

4.1. Forest Decline, Recovery Cycles, and Landscape Transformation

The long-term land cover dynamics in ENFR reveal a landscape undergoing progressive structural transformation driven by the interaction of anthropogenic pressures and environmental variability [88–92]. The continuous decline of dense woodland between 1995 and 2021, coupled with the expansion of semi-bare land, indicates a persistent trajectory toward ecosystem degradation typical of semi-arid savanna systems. This pattern reflects a shift from structurally complex vegetation to simplified and fragmented landscapes, consistent with degradation pathways reported in comparable dryland ecosystems [14,16,35,65,66,93].

Although partial recovery of open woodland was observed after 2008, alongside a reduction in bare land between 2008 and 2021, these improvements were spatially limited and insufficient to offset the overall decline in dense woodland. Such localized recovery is characteristic of semi-arid environments, where regeneration occurs opportunistically under reduced disturbance or favorable micro-site conditions, as documented in previous remote sensing–based studies [43,45,47]. However, the dominance of transitions from dense and open woodland to semi-bare land indicates that degradation processes remain more persistent than recovery dynamics.

The extremely low persistence of dense woodland in certain areas (<1% of its original extent) highlights severe canopy loss and fragmentation. This reflects a breakdown in structural integrity and suggests that ecological thresholds may be approaching, beyond which natural recovery becomes increasingly constrained. Similar transitions have been described as early-stage collapse dynamics in dryland woodlands exposed to sustained disturbance and climatic stress [11,22,26,51,94,95]. Overall, these findings indicate that ENFR is undergoing progressive fragmentation and structural simplification, with increasing vulnerability to further degradation.

4.2. Anthropogenic and Environmental Drivers of Degradation

The findings of this study demonstrate that woodland degradation in the Elnour Natural Forest Reserve (ENFR) is primarily driven by anthropogenic pressures, with environmental factors acting as secondary but reinforcing stressors. The dominance of human-induced drivers identified in this study is consistent with broader patterns reported across semi-arid ecosystems in Sudan and sub-Saharan Africa [16,35,65,66].

Illegal tree cutting and charcoal production emerged as the most influential drivers of woodland degradation. These activities are closely linked to increasing urban energy demand and limited alternative livelihood options, leading to intensified extraction beyond subsistence levels. Similar findings have been widely reported in dryland regions, where charcoal production is a major contributor to canopy loss and structural degradation of woodland ecosystems [16,35,65,66]. The removal of mature trees not only reduces biomass but also disrupts regeneration processes, resulting in long-term declines in woodland resilience.

Overgrazing was identified as another critical driver influencing woodland dynamics. Continuous livestock movement within and around ENFR limits seedling establishment and alters species composition, favoring disturbance-tolerant species. This pattern aligns with previous studies demonstrating that grazing pressure in semi-arid environments creates persistent regeneration bottlenecks and inhibits woodland recovery [13,18,54,94,96]. The combined effect of tree removal and grazing pressure accelerates the transition from dense woodland to more open and degraded land cover types.

Governance-related constraints further intensify these processes. Weak institutional enforcement, unclear land tenure systems, and limited management capacity reduce the effectiveness of conservation measures and enable unsustainable resource use. This finding is consistent with regional studies highlighting governance limitations as a key underlying driver of land degradation in dryland systems [17].

Socioeconomic dependence on woodland resources also plays a significant role. Local communities rely heavily on fuelwood, charcoal production, and grazing for their livelihoods, particularly in contexts of economic instability and low agricultural productivity. This dependence reinforces extraction pressures and limits the adoption of sustainable resource management practices, as reported in similar socio-ecological systems [14].

Although environmental factors such as prolonged dry seasons and rainfall variability were found to have a comparatively lower direct influence, they play an important role in shaping ecosystem response. Climatic stress reduces seedling survival, limits vegetation recovery, and increases the vulnerability of already degraded woodland areas. These interactions highlight the role of climate as a stress multiplier that amplifies the impacts of human activities rather than acting as an independent primary driver.

Overall, the interaction between anthropogenic pressures and environmental variability creates a reinforcing cycle of degradation in ENFR. This coupled human–environment system leads to progressive woodland fragmentation, shifts in species composition, and the expansion of degraded land cover types. Such dynamics are consistent with patterns observed in other semi-arid woodland ecosystems, where the combined effects of resource extraction, grazing pressure, and climatic stress drive long-term landscape transformation [16,65,66,97].

4.3. Ecological Implications of Historical and Future LC Change

The observed historical and projected land cover dynamics have important ecological implications for ENFR. The decline of dense woodland reduces habitat availability, disrupts ecological connectivity, and limits the persistence of key functional species that sustain

ecosystem processes in dryland environments. These changes weaken ecosystem stability and reduce resilience to external disturbances.

The expansion of semi-bare land reflects a transition toward degraded states characterized by increased soil exposure, reduced vegetation cover, and higher susceptibility to erosion. This pattern is consistent with ecological degradation trajectories reported in semi-arid landscapes, where repeated disturbance leads to reduced regenerative capacity and shifts toward low-productivity vegetation mosaics [13,18,54,96,97]. The persistence of semi-bare land suggests that portions of the landscape may be approaching a stable degraded equilibrium, where natural recovery is limited without external intervention.

Future projections indicate a moderate increase in dense woodland; however, this recovery remains spatially constrained and does not fully compensate for historical losses. The relative stability of open woodland suggests that this class functions as a transitional state, mediating shifts between dense vegetation and degraded land cover. Similar transitional dynamics have been reported in other dryland systems, where intermediate canopy cover plays a critical role in regulating ecosystem responses to disturbance [43,45,66,94].

Despite indications of partial recovery, the continued dominance of semi-bare land and fluctuating bare land highlights the persistence of degradation processes. These findings suggest that ENFR is transitioning toward a more fragmented and less resilient ecosystem, consistent with landscape patterns observed in other semi-arid woodland environments [47,83].

4.4. Interpretation of Future Landscape Stability and Vulnerability

The CA–ANN-based projections provide insights into the balance between recovery potential and ongoing vulnerability in ENFR. The persistence of semi-bare land across future scenarios indicates that degraded states may become increasingly stable over time, particularly in the absence of active management interventions. This aligns with regional studies showing that semi-bare land often represents a critical ecological bottleneck limiting woodland recovery in semi-arid environments [54,83,93,96,97].

The projected increase in dense woodland suggests that certain areas retain the capacity for regeneration, likely due to localized reductions in disturbance or favorable environmental conditions. However, this recovery is uneven and does not represent a system-wide reversal of degradation trends. Similar patterns have been reported in dryland forests, where recovery occurs in patches rather than across the entire landscape [11,16,55,95].

The gradual transition of bare land into vegetated classes in future scenarios indicates potential for passive restoration [53,83,98]. However, the long-term stability of open woodland further emphasizes its role as an intermediate state controlling transitions between degraded and dense vegetation. These dynamics highlight the importance of spatial heterogeneity in shaping landscape trajectories [14,35,66].

Overall, the projections indicate that ENFR remains vulnerable to continued degradation under current conditions. The coexistence of localized recovery and widespread degradation reflects a system operating near critical thresholds, where small changes in disturbance regimes or climate conditions may lead to disproportionate landscape responses. This reinforces the need for targeted interventions to shift the system toward more stable and resilient states.

4.5. Management and Policy Recommendations for ENFR

The observed land cover dynamics highlight the need for targeted and integrated management strategies to enhance ecosystem resilience in ENFR. Given the dominant role of anthropogenic drivers, strengthening forest governance is essential. Improved enforcement mechanisms, participatory management approaches, and clear land tenure

systems can reduce uncontrolled resource extraction, as demonstrated in similar dryland contexts [16,18,66,88,94].

Reducing pressure on woodland resources requires diversification of livelihoods and the promotion of alternative energy sources to decrease dependence on charcoal production. Restoration efforts should prioritize semi-bare land areas, which represent the most persistent degraded class, through interventions such as assisted natural regeneration, enrichment planting, and controlled grazing management [18,54,65,66,96].

The relative stability of open woodland suggests that it represents a strategic target for restoration, where interventions can enhance recovery trajectories. In addition, improving agricultural productivity outside of forest areas may reduce expansion pressure on woodland margins.

Continuous monitoring of land cover dynamics is essential for adaptive management. Remote sensing–based approaches provide valuable tools for tracking changes and identifying emerging degradation hotspots, supporting evidence-based decision making in data-limited environments [14,35,45,75].

4.6. Limitations and Uncertainty of the CA–ANN Modeling Approach

While the CA–ANN framework provides a robust basis for simulating future land cover dynamics in ENFR, several sources of uncertainty influence the reliability of long-term projections.

First, uncertainty arises from input data quality, including the spatial resolution, temporal consistency, and representativeness of historical land cover maps and driving variables. Errors or inconsistencies in these inputs may propagate through the modeling process and affect the stability of simulated outcomes [51,52,99].

Second, the CA–ANN model assumes temporal stationarity, whereby historical transition patterns and relationships between land cover change and driving factors remain constant over time. However, rapid socio-economic or governance changes, such as fluctuations in charcoal demand, shifts in grazing intensity, or expansion of agricultural activities, may alter these relationships, thereby reducing the predictive reliability of long-term simulations [83,97,100].

Third, model outputs are sensitive to parameterization, including neighborhood configuration, transition thresholds, and the relative influence of driving variables. Variations in these parameters can affect both the magnitude and spatial allocation of simulated land cover transitions, particularly in ecotonal zones such as woodland, semi-bare land interfaces [51,101].

Fourth, certain drivers of land cover change are difficult to quantify or were not explicitly included in the modeling framework. Factors such as informal resource extraction, variability in policy enforcement, extreme climatic events (e.g., drought), and conflict-induced population displacement may lead to abrupt or non-linear changes that are not fully captured by the model.

Finally, uncertainty increases with the projection horizon. While the CA–ANN model demonstrates reliable performance for short- to medium-term simulations, projections extending beyond two decades inherently accumulate uncertainty. Therefore, the projected land cover patterns for 2047 and 2060 should be interpreted as plausible scenario-based outcomes rather than precise predictions, particularly in semi-arid ecosystems characterized by high environmental variability and socio-economic sensitivity [52,97,99,101,102].

In addition to the qualitative assessment of uncertainty, model reliability was evaluated through comparison between the simulated and observed 2021 land cover maps (Figure 10). The results demonstrate a strong level of spatial agreement for dominant classes such as Semi-bare land and Open Woodland, indicating that the model effectively captures

the overall landscape structure. However, discrepancies observed in transition zones, particularly between Open Woodland and Semi-bare land, highlight areas of higher uncertainty associated with localized land cover dynamics and classification sensitivity. These findings reinforce that the CA–ANN projections should be interpreted as scenario-based outcomes rather than exact predictions.

5. Conclusions

This study demonstrates a clear long-term transition in the ENFR from dense woodland to predominantly lower-density and degraded land cover classes over the period 1995–2021. The results indicate a continuous decline in dense woodland, a substantial expansion of semi-bare land, and limited persistence of intact vegetation, reflecting significant structural transformation of the landscape. Future projections based on the CA–ANN framework suggest partial recovery of dense woodland; however, semi-bare land is expected to remain the dominant class through 2060, indicating continued ecosystem vulnerability.

By integrating multi-temporal classification using the Random Forest algorithm with spatially explicit CA–ANN modeling, this study provides a comprehensive assessment of both historical land cover dynamics and potential future trajectories in a semi-arid woodland environment. The findings highlight the persistence of degradation patterns alongside localized recovery processes, emphasizing the complexity of landscape dynamics in dryland ecosystems.

The study contributes to land cover research by demonstrating the applicability of combining machine learning classification and spatial simulation approaches for analyzing long-term changes and projecting future scenarios in data-limited regions. This integrated framework improves understanding of land cover transitions and provides a basis for evaluating potential future landscape conditions.

Future research should incorporate additional socio-ecological variables, such as spatially explicit grazing intensity, resource extraction patterns, and local land-use practices, to improve model representation of driving processes. The application of multi-model approaches and higher-resolution datasets may further enhance the robustness of projections and reduce uncertainty. In addition, field-based observations of vegetation structure, regeneration dynamics, and soil conditions are needed to support model calibration and validation.

Overall, advancing integrated approaches that combine remote sensing, spatial modeling, and socio-ecological analysis will be essential for improving the assessment and monitoring of land cover dynamics in semi-arid woodland ecosystems.

Author Contributions: Conceptualization, E.H.E.Y.; methodology, E.H.E.Y.; validation, E.H.E.Y.; formal analysis, E.H.E.Y.; investigation, E.H.E.Y.; data curation, E.H.E.Y.; writing—original draft preparation, E.H.E.Y.; writing—review and editing, E.H.E.Y. and M.K.; visualization, E.H.E.Y. and M.K.; supervision, M.K. and K.C. All authors have read and agreed to the published version of the manuscript.

Funding: This research received funds from the project TKP2021-NVA-13 which has been implemented with the support provided by the Ministry of Culture and Innovation of Hungary from the National Research, Development and Innovation Fund, financed under the TKP2021-NVA funding scheme.

Data Availability Statement: The data that support the findings of this study are available from the corresponding author upon reasonable request.

Acknowledgments: The authors gratefully acknowledge the colleagues and staff of the Institute of Geomatics and Civil Engineering at the University of Sopron for academic collaboration and support, and my colleagues, for their valuable support. Special thanks are extended to the Stipendium Hungaricum for providing scholarship for the first author, the project TKP2021-NVA-13 for providing financial support for the publication of this paper and the Department of Forest Resources Planning and Informatics, Technical University in Zvolen for their support and academic collaboration.

Conflicts of Interest: The authors declare no conflicts of interest.

Abbreviations

The following abbreviations are used in this manuscript:

LC	Land Cover
ENFR	Elnour Natural Forest Reserve
FAO	Food and Agriculture Organization
FRA	Forest Resources Assessment
RF	Random Forest
CA	Cellular Automata
ANN	Artificial Neural Network
CA-ANN	Cellular Automata–Artificial Neural Network
GEE	Google Earth Engine
GIS	Geographic Information System
TM	Thematic Mapper
OLI	Operational Land Imager
MSI	Multi-Spectral Instrument
QGIS	Quantum Geographic Information System
MOLUSCE	Modules for Land Use Change Evaluation
LCC	Land Cover Change
OA	Overall Accuracy
PA	Producer's Accuracy
QD	Quantity Disagreement
AD	Allocation Disagreement
ANR	Assisted Natural Regeneration
UA	User's Accuracy
UAV	Unmanned Aerial Vehicle
PLUS	Patch-generating Land Use Simulation
GEDI	Global Ecosystem Dynamics Investigation

Appendix A

Table A1. Training and Testing Samples.

Class	Training Samples (70%)			Testing Samples (30%)		
	1995	**2008**	**2021**	**1995**	**2008**	**2021**
Bare land	33	135	28	14	58	12
Semi-bare land	148	193	256	64	83	110
Open Woodland	289	157	256	124	67	110
Dense Woodland	171	156	101	73	67	43

Table A2. Accuracy assessment of classified images for 1995, 2008, and 2021.

Year	Class Name	Bare Land	Semi-Bare Land	Open Forest	Dense Forest	Total	UA %	PA %	OA %	Kappa %
1995	Bare land	12	1	1	0	14	75	85.71	89	83.81
	Semi-bare land	1	58	3	2	64	90.63	90.63		
	Open Woodland	2	4	110	8	124	91.67	88.71		
	Dense Woodland	1	1	6	65	73	86.67	89.04		
	Total	16	64	120	75	275				
2008	Bare land	52	3	2	1	58	90.63	89.66	91.6	88
	Semi-bare land	77	3	2	1	83	93.9	92.77		
	Open Woodland	1	2	62	2	67	92.54	92.54		
	Dense Woodland	1	1	4	61	67	94.53	91.04		
	Total	82	58	70	65	275				
2021	Bare land	11	1	0	0	12	91.67	91.67	93.02	93.6
	Semi-bare land	1	105	3	1	110	96.32	95.45		
	Open Woodland	0	2	106	2	110	95.45	96.36		
	Dense Woodland	0	1	2	40	43	93.02	93.02		
	Total	12	109	111	43	275				

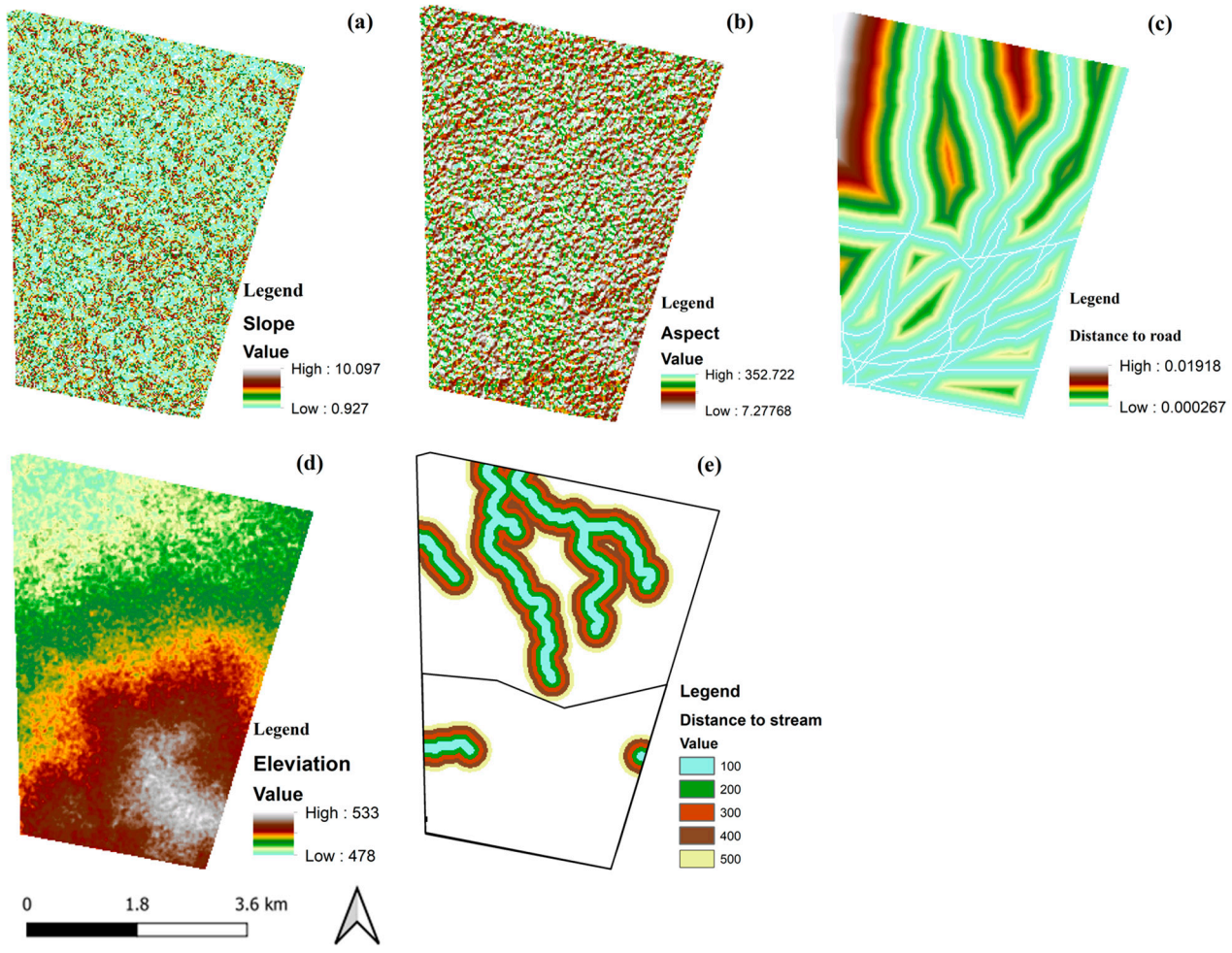

Figure A1. Predictor variables used for land and cover (LC) future prediction including (**a**) slope, (**b**) aspect, (**c**) distance to road, (**d**) elevation, and (**e**) distance to stream. Color gradients represent variable magnitudes, as indicated in the legends.

References

1. FAO. *Trees, Forests and Land Use in Drylands: The First Global Assessment*; FAO: Rome, Italy, 2016.
2. Tolessa, T.; Senbeta, F.; Kidane, M. The impact of land use/land cover change on ecosystem services in the Central Highlands of Ethiopia. *Ecosyst. Serv.* **2017**, *23*, 47–54. [CrossRef]
3. Osewe, E.O.; Popa, B.; Vacik, H.; Osewe, I.; Abrudan, I.V. Review of forest ecosystem services evaluation studies in East Africa. *Front. Ecol. Evol.* **2024**, *12*, 1385351. [CrossRef]
4. Bourgoin, C.; Ceccherini, G.; Girardello, M.; Vancutsem, C.; Avitabile, V.; Beck, P.S.A.; Vieilledent, G. Human degradation of tropical moist forests is greater than previously estimated. *Nature* **2024**, *631*, 570–576. [CrossRef]
5. Biro, K.; Pradhan, B.; Buchroithner, M.; Makeschin, F. Land use/land cover change analysis and its impact on soil properties in the northern part of Gadarif region, Sudan. *Land Degrad. Dev.* **2013**, *24*, 90–102. [CrossRef]
6. Winkler, K.; Fuchs, R.; Rounsevell, M.; Herold, M. Global land use changes are four times greater than previously estimated. *Nat. Commun.* **2021**, *12*, 2501. [CrossRef] [PubMed]
7. Mohmmed, A.; Li, J.; Elaru, J.; Elbashier, M.M.A.; Keesstra, S.; Artemi, C. Assessing drought vulnerability and adaptation among farmers in Gadaref region, eastern Sudan. *Land Use Policy* **2018**, *70*, 402–413. [CrossRef]
8. Osman, M.; Yasin, E.H.E. Fostering environmental and resources management in Sudan through geo-information systems: A prospective approach for sustainability. *J. Degrad. Min. Lands Manag.* **2024**, *11*, 5647–5657. [CrossRef]
9. Fonseka, H.P.U.; Zhang, H.; Sun, Y.; Su, H.; Lin, H.; Lin, Y. Urbanization and its impacts on land surface temperature in Colombo Metropolitan Area, Sri Lanka, from 1988 to 2016. *Remote Sens.* **2019**, *11*, 957. [CrossRef]
10. Nath, B.; Niu, Z.; Singh, R.P. Land use and land cover changes, and environment and risk evaluation of Dujiangyan city (SW China) using remote sensing and GIS techniques. *Sustainability* **2018**, *10*, 4631. [CrossRef]
11. Zhang, B.; Zhang, Q.; Feng, C.; Feng, Q.; Zhang, S. Understanding land use and land cover dynamics from 1976 to 2014 in Yellow River Delta. *Land* **2017**, *6*, 20. [CrossRef]
12. Lin, S.; Fan, C.; Wang, J.; Zhang, C.; Zhao, X.; Wang, S. Spatio-temporal dynamics and driving factors of forest cover changes in the Mekong River Basin. *Forests* **2023**, *14*, 1601. [CrossRef]
13. Husar, M.; Hajduk, J.; Ondrejicka, V. GIS-based decision support tool for evidence-based policy making for biodiversity protection. *MATEC Web Conf.* **2024**, *396*, 19003. [CrossRef]
14. Tamiminia, H.; Salehi, B.; Mahdianpari, M.; Quackenbush, L.; Adeli, S.; Brisco, B. Google Earth Engine for geo-big data applications: A meta-analysis and systematic review. *ISPRS J. Photogramm. Remote Sens.* **2020**, *164*, 152–170. [CrossRef]
15. de Almeida, D.R.; Vedovato, L.B.; Fuza, M.; Molin, P.; Cassol, H.; Resende, A.F.; Krainovic, P.M.; de Almeida, C.T.; Amaral, C.; Haneda, L.; et al. Remote sensing approaches to monitor tropical forest restoration: Current methods and future possibilities. *J. Appl. Ecol.* **2025**, *62*, 188–206. [CrossRef]
16. Sulieman, H.M. Exploring drivers of forest degradation and fragmentation in Sudan: The case of Erawashda Forest and its surrounding community. *Sci. Total Environ.* **2018**, *621*, 895–904. [CrossRef]
17. Munthali, M.G.; Davis, N.; Adeola, A.M.; Botai, J.O.; Kamwi, J.M.; Chisale, H.L.W. Local perception of drivers of land-use and land-cover change dynamics across Dedza District, Central Malawi region. *Sustainability* **2019**, *11*, 832. [CrossRef]
18. Gadallah, N.A.H.; Hano, A.; Yagoub, Y. Characterizing forest cover changes based on satellite images cum forest dependents' data. *Agric. For. J.* **2020**, *4*, 63–70. [CrossRef]
19. Midekisa, A.; Holl, F.; Savory, D.J.; Andrade Pacheco, R.; Gething, P.W.; Bennett, A. Mapping land cover change over continental Africa using Landsat and Google Earth Engine cloud computing. *PLoS ONE* **2017**, *12*, e0184926. [CrossRef]
20. Siddig, A.A. Why is biodiversity data deficiency an ongoing conservation dilemma in Africa? *J. Nat. Conserv.* **2019**, *50*, 125719. [CrossRef]
21. Dubovik, O.; Schuster, G.L.; Xu, F.; Hu, Y.; Bösch, H.; Landgraf, J. Grand challenges in satellite remote sensing. *Front. Remote Sens.* **2021**, *2*, 619818. [CrossRef]
22. Hasoba, A.M.M.; Siddig, A.A.H.; Yagoub, Y.E. Exploring tree diversity and stand structure of savanna woodlands in southeastern Sudan. *J. Arid Land* **2020**, *12*, 609–617. [CrossRef]
23. Siddig, A.A. Biodiversity of Sudan: Between the harsh conditions, political instability and civil wars. *Biodivers. J.* **2014**, *5*, 545–555.
24. Eltohami, A.B.E.S.A. Threats to green gum arabic production in Sudan. *Biomed. J. Sci. Tech. Res.* **2018**, *3*, 3526–3530. [CrossRef]
25. Gurashi, N.A.; Yasin, E.H.; Czimber, K. Assessment of tree species availability based on sawmilling and timber markets survey in Sinnar State, Sudan. *Acta Silv. Lignaria Hung.* **2024**, *20*, 39–51. [CrossRef]
26. Yasin, E.H.E.; Mulyana, B. Spatial distribution of tree species composition and carbon stock in Tozi tropical dry forest, Sinnar State, Sudan. *Biodiversitas* **2022**, *23*, 2359–2368. [CrossRef]
27. Glover, E.K.; Elsiddig, E.A. The causes and consequences of environmental changes in Gedaref, Sudan. *Land Degrad. Dev.* **2012**, *23*, 339–349. [CrossRef]
28. Hano, A.I. Assessment of Impacts of Changes in Land Use Patterns on Land Degradation/Desertification in the Semi-Arid Zone of White Nile State, Sudan, by Means of Remote Sensing and GIS. Ph.D. Thesis, TU Dresden, Dresden, Germany, 2013.

29. Sulieman, H.M.; Ahmed, A.G.M. Monitoring changes in pastoral resources in eastern Sudan: A synthesis of remote sensing and local knowledge. *Pastoralism* **2013**, *3*, 22. [CrossRef]
30. Idreas, A.E.L.A. Effect of Mechanized Rain-Fed Farming on Vegetation Cover and Effect of Shelter Belts on Environment at Ghadambaliya Area Gedaref State (Sudan). Ph.D. Thesis, Sudan University of Science and Technology, Khartoum, Sudan, 2015.
31. Adam, M.I.A. Assessment of El-Rawashda Reserved Forest Resources Using Selected Climate Change Indicators, Gedaref State, Sudan. Master's Thesis, Sudan University of Science and Technology, Khartoum, Sudan, 2019.
32. Yasin, E.H.; Kornel, C.; Hemida, M. Assessment and mapping of forest cover change in dryland, Sudan using remote sensing. In *Conservation, Exploitation and Restoration of Mountain Ecosystem*; IntechOpen: London, UK, 2023; pp. 65–79. [CrossRef]
33. Hemida, M.; Yasin, E.H.E.; Kheiry, M.A.; Hammad, Z.M.; Vityi, A. Assessment of Taungya agroforestry system in dryland forests rehabilitation in Sudan. *J. Degrad. Min. Lands Manag.* **2023**, *10*, 4495–4507. [CrossRef]
34. FAO. *Global Forest Resources Assessment 2015: How Are the World's Forests Changing?* FAO: Rome, Italy, 2015. Available online: https://www.fao.org/forest-resources-assessment/ (accessed on 20 November 2025).
35. Gorelick, N.; Hancher, M.; Dixon, M.; Ilyushchenko, S.; Thau, D.; Moore, R. Google Earth Engine: Planetary-scale geospatial analysis for everyone. *Remote Sens. Environ.* **2017**, *202*, 18–27. [CrossRef]
36. Potapov, P.; Hansen, M.C.; Pickens, A.; Hernandez-Serna, A.; Tyukavina, A.; Turubanova, S. The global 2000–2020 land cover and land use change dataset derived from the Landsat archive: First results. *Front. Remote Sens.* **2022**, *3*, 856903. [CrossRef]
37. Brown, C.F.; Brumby, S.P.; Guzder-Williams, B.; Birch, T.; Hyde, S.B.; Mazzariello, J. Dynamic World, near real-time global 10 m land use land cover mapping. *Sci. Data* **2022**, *9*, 251. [CrossRef]
38. Tesfaye, W.; Elias, E.; Warkineh, B.; Tekalign, M.; Abebe, G. Modeling of land use and land cover changes using Google Earth Engine and machine learning approach: Implications for landscape management. *Environ. Syst. Res.* **2024**, *13*, 31. [CrossRef]
39. De Sousa, C.; Fatoyinbo, L.; Neigh, C.; Boucka, F.; Angoue, V.; Larsen, T. Cloud-computing and machine learning in support of country-level land cover and ecosystem extent mapping in Liberia and Gabon. *PLoS ONE* **2020**, *15*, e0227438. [CrossRef]
40. Griffiths, P.; van der Linden, S.; Kuemmerle, T.; Hostert, P. A pixel-based Landsat compositing algorithm for large area land cover mapping. *IEEE J. Sel. Top. Appl. Earth Obs. Remote Sens.* **2013**, *6*, 1939–1944. [CrossRef]
41. Hermosilla, T.; Wulder, M.A.; White, J.C.; Coops, N.C.; Hobart, G.W. An integrated Landsat time series protocol for change detection and generation of annual gap free surface reflectance composites. *Remote Sens. Environ.* **2015**, *158*, 220–234. [CrossRef]
42. Breiman, L. Random forests. *Mach. Learn.* **2001**, *45*, 5–32. [CrossRef]
43. Pelletier, C.; Valero, S.; Inglada, J.; Champion, N.; Dedieu, G. Assessing the robustness of Random Forests to map land cover with high-resolution satellite image time series over large areas. *Remote Sens. Environ.* **2016**, *187*, 156–168. [CrossRef]
44. Feng, W.; Ma, C.; Zhao, G.; Zhang, R. FSRF: An improved random forest for classification. In Proceedings of the IEEE International Conference on Advanced Electrical Engineering and Computer Applications, Dalian, China, 25–27 August 2020; pp. 173–178. [CrossRef]
45. Phan, N.T.; Kuch, V.; Lehnert, L.W. Land cover classification using Google Earth Engine and Random Forest classifier—The role of image composition. *Remote Sens.* **2020**, *12*, 2411. [CrossRef]
46. Ghimire, B.; Rogan, J.; Galiano, V.; Panday, P.; Neeti, N. An evaluation of bagging, boosting, and random forests for land-cover classification in Cape Cod, Massachusetts, USA. *GISci. Remote Sens.* **2012**, *49*, 623–643. [CrossRef]
47. Zurqani, H.A.; Post, C.J.; Mikhailova, E.A.; Schlautman, M.A.; Sharp, J.L. Geospatial analysis of land use change in the Savannah River Basin using Google Earth Engine. *Int. J. Appl. Earth Obs. Geoinf.* **2018**, *69*, 175–185. [CrossRef]
48. Aldwaik, S.Z.; Pontius, R.G. Intensity analysis to unify measurements of size and stationarity of land changes by interval, category, and transition. *Landsc. Urban Plan.* **2012**, *106*, 103–114. [CrossRef]
49. Zhou, P.; Huang, J.; Pontius, R.G.; Hong, H. Land classification and change intensity analysis in a coastal watershed of Southeast China. *Sensors* **2014**, *14*, 11640–11658. [CrossRef] [PubMed]
50. Gounaridis, D.; Chorianopoulos, I.; Symeonakis, E.; Koukoulas, S. A random forest-cellular automata modelling approach to explore future land use/cover change in Attica (Greece), under different socio-economic realities and scales. *Sci. Total Environ.* **2019**, *646*, 320–335. [CrossRef]
51. Basse, R.M.; Omrani, H.; Charif, O.; Gerber, P.; Bodis, K. Land use changes modelling using advanced methods: Cellular automata and artificial neural networks. *Appl. Geogr.* **2014**, *53*, 160–171. [CrossRef]
52. Qiang, Y.; Lam, N.S.N. Modeling land use and land cover changes in a vulnerable coastal region using artificial neural networks and cellular automata. *Environ. Monit. Assess.* **2015**, *187*, 57. [CrossRef]
53. Saputra, M.H.; Lee, H.S. Prediction of land use and land cover changes for North Sumatra, Indonesia, using an artificial-neural-network-based cellular automaton. *Sustainability* **2019**, *11*, 3024. [CrossRef]
54. Haq, B.; Jamshed, M.A.; Ali, K.; Kasi, B.; Arshad, S.; Kasi, M.K.; Ali, I.; Shabbir, A.; Abbasi, Q.H.; Ur-Rehman, M. Tech-driven forest conservation: Combating deforestation with Internet of Things, artificial intelligence, and remote sensing. *IEEE Internet Things J.* **2024**, *11*, 24551–24568. [CrossRef]

55. Baig, M.F.; Mustafa, M.R.U.; Baig, I.; Takaijudin, H.B.; Zeshan, M.T. Assessment of land use land cover changes and future predictions using CA–ANN simulation for Selangor, Malaysia. *Water* **2022**, *14*, 402. [CrossRef]
56. Buğday, E.; Erkan Buğday, S. Modeling and simulating land use/cover change using artificial neural network from remotely sensing data. *Cerne* **2019**, *25*, 246–254. [CrossRef]
57. Kafy, A.A.I.; Naim, M.N.H.; Subramanyam, G.; Faisal, A.A.I.; Ahmed, N.U.; Rakib, A.A.I. Cellular automata approach in dynamic modelling of land cover changes using RapidEye images in Dhaka, Bangladesh. *Environ. Chall.* **2021**, *4*, 100084. [CrossRef]
58. Muhammad, R.; Zhang, W.; Abbas, Z.; Guo, F.; Gwiazdzinski, L. Spatiotemporal change analysis and prediction of future land use and land cover changes using QGIS MOLUSCE plugin and remote sensing big data: A case study of Linyi, China. *Land* **2022**, *11*, 419. [CrossRef]
59. Gismondi, M. MOLUSCE, an Open-Source Land Use Change Analyst. Presented at FOSS4G Conference 2013. Available online: https://2013.foss4g.org/conf/programme/presentations/107/ (accessed on 30 December 2025).
60. Tripathi, K.; Verma, A. Remote sensing and machine learning fusion: A robust framework for land use and land cover change detection. In Proceedings of the 2024 IEEE International Conference for Women in Innovation, Technology & Entrepreneurship (ICWITE), Bangalore, India, 16–17 February 2024; pp. 434–439. [CrossRef]
61. Mohamed, M.S.D. Mapping and Assessment of Land Use/Land Cover Using Remote Sensing and GIS in North Kordofan State, Sudan. Ph.D. Thesis, Dresden University of Technology, Dresden, Germany, 2006.
62. Zakaria, H.E.A. Integration of Remote Sensing and GIS in Studying Vegetation Trends and Conditions in the Gum Arabic Belt in North Kordofan, Sudan. Ph.D. Thesis, Technical University of Dresden, Dresden, Germany, 2010.
63. Dafalla, M.S.; Abdel Rahman, E.M.; Siddig, K.H.A.; Ibrahim, I.S.; Csaplovics, E. Land use and land cover changes in Northern Kordofan State of Sudan: A remotely sensed data analysis. In *Nile River Basin*; Melesse, A.M., Setegn, W.W.S., Eds.; Springer: Cham, Switzerland, 2014; pp. 269–283.
64. Sulieman, H.M. Expansion of mechanised rain fed agriculture and land use/land cover change in southern Gadarif, Sudan. *Afr. J. Agric. Res.* **2010**, *5*, 1609–1615. [CrossRef]
65. Yasin, E.H.; Kamil, O.H.; Mulyana, B. Multi-temporal satellite images analysis for assessing and mapping deforestation in Um Hataba Forest, South Kordofan, Sudan. *J. Sylva Indones.* **2022**, *5*, 81–92. [CrossRef]
66. Yasin, E.H.; Siddig, A.A.; Diab, E.E.; Czimber, K. Evaluating the efficiency of two ecological indices in monitoring forest degradation in the drylands of Sudan. *Remote Sens.* **2025**, *17*, 2298. [CrossRef]
67. Harrison, M.N.; Jackson, J.K. *Ecological Classification of Vegetation*; Sudan Agricultural Publications Committee: Khartoum, Sudan, 1958.
68. Ibrahim, E.; Osman, E.; Idris, E. Modelling the relationship between crown width and diameter at breast height for naturally grown *Terminalia* tree species. *J. Nat. Resour. Environ. Stud.* **2014**, *6456*, 42–49.
69. Ibrahim, E.M.I.; Osman, E.H. Diameter at breast height–crown width prediction models for *Anogeissus leiocarpus* (DC.) Guill. & Perr. and *Combretum hartmannianum* Schweinf. *J. For. Prod. Ind.* **2014**, *3*, 191–197.
70. Gibreel, H.H.; Kordofani, M.A.I.; Warrag, E.I.; Ahmed, H.O. Medicinal value and eco-taxonomy of the flora of Blue Nile State-Sudan. *J. Chem. Pharm. Res.* **2013**, *5*, 36–43.
71. Fahmi, M.K.M. Climate, Trees and Agricultural Practices: Implications for Food Security in the Semi-Arid Zone of Sudan. In *Tropical Forestry Reports*; University of Helsinki, Tropical Forestry Department: Helsinki, Finland, 2017.
72. Qu, L.; Chen, Z.; Li, M.; Zhi, J.; Wang, H. Accuracy improvements to pixel-based and object-based LULC classification with auxiliary datasets from Google Earth Engine. *Remote Sens.* **2021**, *13*, 453. [CrossRef]
73. Hansen, M.C.; Roy, D.P.; Lindquist, E.; Adusei, B.; Justice, C.O.; Altstatt, A. A method for integrating MODIS and Landsat data for systematic monitoring of forest cover and change in the Congo Basin. *Remote Sens. Environ.* **2008**, *112*, 2495–2513. [CrossRef]
74. Lin, L.; Hao, Z.; Post, C.J.; Mikhailova, E.A.; Yu, K.; Yang, L. Monitoring land cover change on a rapidly urbanizing island using Google Earth Engine. *Appl. Sci.* **2020**, *10*, 7336. [CrossRef]
75. Tong, X.; Brandt, M.; Hiernaux, P.; Herrmann, S.; Rasmussen, L.V.; Rasmussen, K.; Tian, F.; Tagesson, T.; Zhang, W.; Fensholt, R. The forgotten land use class: Mapping of fallow fields across the Sahel using Sentinel-2. *Remote Sens. Environ.* **2020**, *239*, 111598. [CrossRef]
76. Ge, Y.; Hu, S.; Ren, Z.; Jia, Y.; Wang, J.; Liu, M. Mapping annual land use changes in China's poverty-stricken areas from 2013 to 2018. *Remote Sens. Environ.* **2019**, *232*, 111285. [CrossRef]
77. Warrens, M.J. Properties of the quantity disagreement and the allocation disagreement. *Int. J. Remote Sens.* **2015**, *36*, 1439–1446. [CrossRef]
78. Foody, G.M. Explaining the unsuitability of the kappa coefficient in the assessment and comparison of the accuracy of thematic maps obtained by image classification. *Remote Sens. Environ.* **2020**, *239*, 111630. [CrossRef]
79. Mudereri, B.T.; Abdel-Rahman, E.M.; Ndlela, S.; Makumbe, L.D.M.; Nyanga, C.C.; Tonnang, H.E.Z.; Mohamed, S.A. Integrating the strength of multi-date Sentinel-1 and Sentinel-2 datasets for detecting mango (*Mangifera indica* L.) orchards in a semi-arid environment in Zimbabwe. *Sustainability* **2022**, *14*, 5741. [CrossRef]

80. Pontius, R.G.; Millones, M. Death to Kappa: Birth of quantity disagreement and allocation disagreement for accuracy assessment. *Int. J. Remote Sens.* **2011**, *32*, 4407–4429. [CrossRef]
81. Anand, V.; Oinam, B. Future land use and land cover prediction with special emphasis on urbanization and wetlands. *Remote Sens. Lett.* **2020**, *11*, 225–234. [CrossRef]
82. Barnieh, B.A.; Jia, L.; Menenti, M.; Zhou, J.; Zeng, Y. Mapping land use and land cover transitions at different spatiotemporal scales in West Africa. *Sustainability* **2020**, *12*, 8565. [CrossRef]
83. Rahman, M.T.U.; Tabassum, F.; Rasheduzzaman, M.; Saba, H.; Sarkar, L.; Ferdous, J.; Uddin, S.Z.; Zahedul Islam, A.Z.M. Temporal dynamics of land use/land cover change and its prediction using CA–ANN model for southwestern coastal Bangladesh. *Environ. Monit. Assess.* **2017**, *189*, 565. [CrossRef]
84. El-Tantawi, A.M.; Bao, A.; Chang, C.; Liu, Y. Monitoring and predicting land use/cover changes in the Aksu Tarim River Basin, Xinjiang-China (1990–2030). *Environ. Monit. Assess.* **2019**, *191*, 480. [CrossRef]
85. Wu, F.; Mo, C.; Dai, X. Analysis of the driving force of land use change based on geographic detection and simulation of future land use scenarios. *Sustainability* **2022**, *14*, 5254. [CrossRef]
86. Hussain, S.; Qaisrani, S.A.; Tariq, A.; Mubeen, M.; Ullah, S. Assessing past, present, and simulated future prediction of land use land cover changes using CA-Markov chain models with satellite data. *Results Eng.* **2025**, *26*, 105585. [CrossRef]
87. Tran, T.V.; Tran, D.X.; Myint, S.W.; Latorre-Carmona, P.; Ho, D.D.; Tran, P.H.; Dao, H.N. Assessing spatiotemporal drought dynamics and its related environmental issues in the Mekong River Delta. *Remote Sens.* **2019**, *11*, 2742. [CrossRef]
88. Arfat, Y. Land Use/Land Cover Change Detection and Quantification: A Case Study in Eastern Sudan. Master's Thesis, Department of Physical Geography, Lund University, Lund, Sweden, 2010.
89. MacDicken, K. Introduction to the changes in global forest resources from 1990 to 2015. *For. Ecol. Manag.* **2015**, *352*, 1–2. [CrossRef]
90. Lambin, E.F.; Geist, H.J.; Lepers, E. Dynamics of land-use and land-cover change in tropical regions. *Annu. Rev. Environ. Resour.* **2003**, *28*, 205–241. [CrossRef]
91. Briones, P.S.; Sepúlveda-Varas, A. Systematic transitions in land use and land cover in a pre-Andean subwatershed with high human intervention in the Araucania Region, Chile. *Int. J. Agric. Nat. Resour.* **2016**, *43*, 396–407.
92. Petit, C.; Scudder, T.; Lambin, E. Quantifying processes of land-cover change by remote sensing: Resettlement and rapid land-cover changes in south-eastern Zambia. *Int. J. Remote Sens.* **2001**, *22*, 3435–3456. [CrossRef]
93. Zewdie, W.; Csaplovics, E. Identifying categorical land use transition and land degradation in northwestern drylands of Ethiopia. *Remote Sens.* **2016**, *8*, 408. [CrossRef]
94. Yasin, E.H.E.; Siddig, A.A.H.; Kornel, C. Forests at the Crossroads: Biodiversity Conservation in the Era of Climate Change. In *Sustainable Forest Management—Surpassing Climate Change and Land Degradation*; Kulshreshtha, S.N., Ed.; IntechOpen: London, UK, 2024. [CrossRef]
95. Mouafik, M.; Chakhchar, A.; Fouad, M.; El Aboudi, A. Remote sensing technologies for monitoring Argane forest stands: A comprehensive review. *Geographies* **2024**, *4*, 441–461. [CrossRef]
96. Sulieman, H.M.; Elagib, N.A. Implications of climate, land-use and land-cover changes for pastoralism in eastern Sudan. *J. Arid Environ.* **2012**, *85*, 132–141. [CrossRef]
97. Abbas, Z.; Yang, G.; Zhong, Y.; Zhao, Y. Spatiotemporal change analysis and future scenario of LULC using the CA-ANN approach: A case study of the Greater Bay Area, China. *Land* **2021**, *10*, 584. [CrossRef]
98. Lambin, E.F.; Meyfroidt, P. Global land use change, economic globalization, and the looming land scarcity. *Proc. Natl. Acad. Sci. USA* **2011**, *108*, 3465–3472. [CrossRef]
99. Phonphan, W.; Arunplod, C.; Wongsongja, N.; Utarasakul, T.; Niemmanee, T.; Kayee, P.; Daraneesrisuk, J.; Thongdara, R. Evaluating spatiotemporal dynamics: A comparative study of predictive efficacy in land use land cover change models—Markov Chain, CA-ANN, and PLUS. *Int. J. Geoinform.* **2024**, *20*, 13–25. [CrossRef]
100. Ouma, Y.O.; Nkwae, B.; Odirile, P.; Moalafhi, D.B.; Anderson, G.; Parida, B.; Qi, J. Land-use change prediction in dam catchment using logistic regression-CA, ANN-CA and random forest regression and implications for sustainable land–water nexus. *Sustainability* **2024**, *16*, 1699. [CrossRef]
101. Li, T.; Li, W. Multiple land use change simulation with Monte Carlo approach and CA-ANN model: A case study in Shenzhen, China. *Environ. Syst. Res.* **2015**, *4*, 1. [CrossRef]
102. Solaimani, K.; Darvishi, S. Comparative analysis of land use changes modeling based on new hybrid models and CA-Markov in the Urmia Lake Basin. *Adv. Space Res.* **2024**, *74*, 3749–3764. [CrossRef]